C.Bedon, M.Fragiacomo (2015). "Numerical and analytical assessment of the buckling behaviour of Blockhaus log-walls under in-plane compression", Engineering Structures, 82(1): 134-150.

Numerical and analytical assessment of the buckling behaviour of *Blockhaus* log-walls under in-plane compression

Chiara Bedon[1]*, Massimo Fragiacomo[2]

Abstract

Blockhaus structural systems are commonly obtained by assembling multiple timber logs, by stacking them horizontally on the top of one another. Although based on simple mechanisms of ancient origins, the structural behaviour of *Blockhaus* systems under well-defined loading and boundary conditions is complex to predict.

The paper focuses on the assessment of the typical buckling behaviour and resistance of vertically compressed timber log-walls. The effects of various mechanical and geometrical variables such as possible load eccentricities and initial curvatures, openings (e.g. doors or windows), fully flexible or in-plane rigid inter-storey floors are investigated by means of detailed finite-element (FE) numerical models. These FE models were first validated on test results of past buckling experiments performed on scaled log-wall specimens, as well as on recent buckling experiments carried out on full-scale timber log-walls, demonstrating the capability to appropriately describe the effective interaction between timber logs and to correctly predict the expected buckling failure mechanisms and ultimate resistance for the log-walls that were investigated. Comparisons with analytical solutions partly derived from classical theory of plate buckling and column buckling are also presented and critically discussed, in order to assess the applicability of these existing formulations – although specific for fully monolithic and isotropic plates and columns – to *Blockhaus* structural systems. A closed-form solution is finally proposed as a simplified design buckling method for timber log-walls under in-plane compression.

Keywords: timber log-walls, buckling; analytical models; finite-element numerical modelling; buckling experiments.

1. Introduction

Blockhaus structural systems represent a construction technology of ancient origins. These structures are commonly obtained by placing a series of timber logs, horizontally on the top of one another, so as to form

[1] Ph.D., Researcher. University of Trieste, Department of Engineering and Architecture, Piazzale Europa 1, 34127 Trieste, Italy. Corresponding author (bedon@dicar.units.it).
[2] Associate Professor. University of Sassari, Department of Architecture, Design and Urban Planning, Piazza Duomo n.6, 07041 Alghero (SS), Italy.

the walls. The interaction between these basic components is provided by simple mechanisms such as simple corner joints and contact surfaces, in order to reduce the use of metal fastener to a minimum.

Despite the ancient origins, *Blockhaus* systems are currently used in modern residential and commercial buildings. At the same time, currently available standards for the design of timber structures do not provide analytical models for an appropriate verification of these structural systems. As a result, the effective structural behaviour and load carrying capacity under specific loading and boundary conditions is complex to predict.

In the last years, only a few studies have been focused on *Blockhaus* structural systems. In [1][2][3] numerical and experimental studies were presented to highlight the typical structural behaviour of timber log-walls under in-plane lateral loads, such as seismic loads. These studies emphasized the high flexibility and damping capability of the system. Earlier studies [4][5] presented a preliminary experimental investigation of log-walls under in-plane vertical loads (Table 1). Buckling experiments were performed on scaled log-wall prototypes, in order to assess their effective buckling resistance under in-plane compressive load.

Buckling phenomena and failure mechanisms, as known, involve in structures a complex interaction between strength and deformation capabilities. In this context, a wide series of experimental research studies and simplified analytical methods are proposed for various structural timber typologies – although not specifically related to log-wall systems – in [6][7][8][9][10][11][12][13].

In this investigation, based on these earlier experimental studies [4][5], as well as on further recent full-scale experiments and numerical investigations using ABAQUS/Standard [6], an assessment of the effective buckling resistance of vertically compressed log-walls is presented. Various geometrical configurations of practical interest are analysed, in order to highlight the effect of several geometrical and mechanical parameters (e.g. number and position of openings, initial curvatures, load eccentricities, different boundary conditions) on their global behaviour under vertical compressive loads. Numerical predictions are also compared to analytical estimations of simple models derived from literature – both from methods specifically developed for timber log-walls under in plane-compression and from classical theory of plate and column buckling – in order to assess their applicability to the studied systems. The final aim of this research project is the derivation of analytical formulations of practical use for the buckling design and verification of vertically loaded log-walls having different mechanical and geometrical properties (e.g. log cross-section, size and location of openings, load eccentricities), as well as restraint conditions (e.g. orthogonal walls, pillars, in-plane rigid diaphragms, etc.).

2. *Blockhaus* structural systems

In current practice [16], the traditional *Blockhaus* log-wall with height H and length L is obtained by assembling a series of spruce logs with strength class C24 according to [15] (Fig.1a). These logs typically have cross-sectional dimensions of depth h by breadth b, with the h/b ratio being between 1.6 and 2. 4, and

are characterized by small protrusions and tongues that are able to provide interlocking with the upper and lower logs (Fig.1b). In *Blockhaus* buildings, the structural interaction between the main perpendicular walls is then provided by appropriate corner joints (Figs.1c and 1d). Permanent gravity loads are transferred onto each main wall by the inter-storey floors (Fig.1e), which typically realize an in-plane rigid diaphragm (e.g. by using OSB panels and timber joists, or glulam panels arranged on their edges) able to restrain the out-of plane deflections of the wall top logs.

Since metal connectors are generally avoided or minimized in these structural systems, the typical *Blockhaus* wall can sustain the vertical loads as far as a minimum level of contact among the logs is guaranteed. At the same time, the very low modulus of elasticity (MOE) of timber in the direction perpendicular to grain makes the usually slender (high H/b ratio) *Blockhaus* walls susceptible to buckling phenomena - unlike other squat structural systems such as masonry or concrete walls characterized by higher MOE and lower H/b ratios.

In this context, it should be in fact noticed that the H/b ratio of some log-walls currently manufactured (for example: the walls produced by Rubner Haus AG Spa [16]) has been recently further increased, by replacing the traditional 90mm×160mm 'Tirol' and 130mm×160mm 'Schweiz' cross-sections (dashed line in Fig.1b) with 80mm×190mm and 120mm×190mm timber log profiles respectively (solid line in Fig.1b). These variations, in conjunction with possible load eccentricities, particular geometrical configurations (e.g. large size walls with door and window openings close to each other and/or to the lateral ends of the wall) or geometrical imperfections (e.g. initial curvatures) could have significant effects on the load-carrying capacity of the studied log-walls, hence requiring careful consideration in their design and verification.

3. Existing analytical models

3.1. Timber log-walls

Over the last decades, only a few studies have been dedicated to the assessment of the buckling behaviour of timber log-walls under in-plane vertical loads. Heimeshoff and Kneidl [4][5] performed a series of experiments on timber log-walls subjected to concentrated mid-span vertical loads N (Fig.2). Buckling experiments were carried-out on 28 specimens (16 (1:4)-scaled specimens (series A) and 12 (1:1.4)-scaled specimens (series B), respectively) characterized by various geometrical configurations (e.g. no openings; single door opening; door and window openings).

The typical specimen consisted of a series of overlapping logs made of spruce, laterally restrained at their ends by means of two short orthogonal log-walls working as outriggers (e.g. Fig.1a) and simply supported at the base. No lateral restraints were introduced at the top log of the main wall (UTL, unrestrained top log), hence suggesting the presence of a fully flexible inter-storey floor enabling possible out-of-plane deformations. Nominal geometrical properties of the tested specimens are schematized in Fig. 2. Buckling experiments on (1:4)-scaled specimens were firstly performed to assess the effects of different timber log cross-sections (e.g. different profiles of grooves along their top and bottom surfaces, Fig.3a), as well as of small load eccentricities (e_{load}= 5mm≈ b/5) on the effective buckling resistance of the studied log-walls.

Preliminary considerations obtained from this first series of experiments were derived from the experimental measurement of the critical buckling load only. Buckling tests on (1:1.4)-scaled specimens were then performed on selected configurations identified within the first series of experiments. During these additional buckling tests, the transversal displacements of specimens were also continuously monitored at seven control points (Fig.3b). For specimens with single door opening, the effects of metal profiles introduced along the vertical edges of openings were also assessed (Fig.3c). As highlighted in [4,5], however, minor resistance improvement was generally found for these specimens, compared to type B02, without metal profiles.

Based on the overall experimental investigation, Heimeshoff and Kneidl also developed simple analytical formulations for the design of log-walls with and without openings, by taking into account the same safety rules of the DIN1052 standard for timber structures [17]. In their theoretical model, the typical log-wall without openings was schematized as a series of horizontal timber logs supported by translational and torsional springs. The buckling problem was then solved by applying the principle of virtual works to a system composed of n bars able to interact together under a concentrated compressive load N. The solution of the corresponding eigenvalue problem lead to the detection of a minimum critical buckling load for the log-wall defined as:

$$\left(N_{cr}\right)_{\min} = \frac{1}{4}c_F h + \frac{c_\varphi}{h}, \tag{1}$$

with the springs elastic constants c_F and c_φ being representative of the flexural and torsional stiffnesses of a single timber log, respectively, calculated as shown in Fig.4, where $E_{||}$ and G signify the MOE in the direction parallel to grain and the shear modulus of timber.

Based on Eq.(1), as result, for a $H \times L$ timber log-wall without openings and composed of $b \times h$ logs, Heimeshoff and Kneidl proposed to estimate the critical buckling load as:

$$N_{cr,0}^{(E)} = \frac{E_{||} b^3 h^2}{L^3} + 0.8\frac{G b^3}{L}. \tag{2}$$

In the case of log-walls with single opening (e.g. $H_d \times L_d$ door, Fig.2a) or double openings (e.g. $H_d \times L_d$ door and $H_w \times L_w$ window), the same authors suggested further simplified analytical formulations derived from Eq.(2), respectively given by:

$$N_{cr,0}^{(E)} = 0.8\frac{G b^3}{L}\left[\frac{H_u}{H} + \frac{H_d}{H}\frac{L - L_d}{L}\right] \tag{3}$$

and

$$N_{cr,0}^{(E)} = 0.8\frac{G b^3}{L}\left[\frac{H_u}{H} + \frac{H_d}{H}\frac{L - \left(L_d + L_i + L_w\right)}{L}\right] + \pi^2 E_\perp \frac{L_i b^3}{48 H^2}. \tag{4}$$

In Eqs.(3) and (4) , $E_\perp$ signifies the MOE of timber in the direction perpendicular to grain, while the dimensions L_d, L_w and L_i - denoting the width of door and window openings, and the distance between them - are given in Fig.2a.

As highlighted in [4][5], Eqs.(2)-(4) can only roughly estimate the Euler's critical load of a log-wall with or without openings under in plane vertical load, as the effects of doors and windows on $N_{cr,0}^{(E)}$ are taken into account in a simplified way. Based on Fig.4b, for example, Eqs.(2)-(4) are accurate only for specific $b \times h$ log cross-sections, since their torsional moment of inertia J_{tor} strictly depends on the h/b ratio, with $h \geq b$, and should be calculated in accordance with [18]:

$$J_{tor} = kb^3 h \cong \frac{1}{3 + 4.1\sqrt{(h/b)^3}} b^3 h . \quad (5)$$

Comparative analytical calculations performed on 'Tirol' and 'Schweiz' timber log profiles currently used in practice by Rubner Haus [16] (Fig. 1b) highlighted for example that the approximate estimation of J_{tor} for a given $b \times h$ log profile can provide discrepancies up to ±25% in the obtained torsional contribution c_φ (Fig. 4b), hence resulting in inaccurate prediction for the corresponding critical load $N_{cr,0}^{(E)}$ (Eqs.(2)-(4)).

Eqs.(3) and (4), moreover, properly account for timber anisotropy, but otherwise consider only the total width of openings – compared to the overall width L – neglecting their position along the width L of the log-wall (e.g. distance of openings from the lateral supports). Finally, the mentioned analytical method strictly applies to log-walls under mid-span concentrated compressive loads N only – rather than to more realistic uniformly distributed compressive loads deriving from inter-storey floors and roofs – and do not take into account the effects of possible load eccentricities e_{load}, as well as initial curvatures u_0 that could affect the overall buckling behaviour of the examined log-walls.

For the above reasons, according to the safety requirements of the DIN standard [17], Heimeshoff and Kneidl proposed a safety factor calibrated on their experimental test results [4][5] and leading to a design buckling resistance:

$$N_{b,Rd} = \frac{N_{cr,0}^{(E)}}{3.5} . \quad (6)$$

3.2. Classical theory of thin plates under in-plane compression

Alternative analytical formulations for the estimation of the buckling resistance $N_{cr,0}^{(E)}$ of timber log-walls under in-plane vertical loads could be taken from the classical theory of thin plates restrained along the four edges and subjected to an in-plane compressive, uniformly distributed compressive pressures q with resultant load N [18]. This approach allows the implementation of the lateral top restraint offered by in-plane rigid floors (RTL, restrained top log). Conversely, the thin plate model does not allow a proper estimation of the interlocking effect between multiple logs, since each log-wall would be regarded as '*fully monolithic*' with thickness b, height H, width L. Assuming for timber an equivalent, isotropic mechanical behaviour, the critical buckling load would in fact be given by [18]:

$$N_{cr,0}^{(E)} = k_\sigma \frac{\pi^2}{12}\frac{E_\perp b^3}{L}\frac{1}{\left(1-\nu_{eq}^2\right)} = k_\sigma \frac{\pi^2}{12}\frac{E_\perp b^3}{L}\frac{1}{\left(1-\left(\frac{E_\perp}{2G}-1\right)^2\right)}, \quad (7)$$

being G the longitudinal shear modulus and ν_{eq} the corresponding Poisson's ratio.

In Eq.(7), k_σ is a buckling coefficient able to take into account the effects of various lateral and top-bottom restraints. Based on the adopted corner joints (Fig.1), k_σ should be in fact calculated as a function of the log-wall aspect ratio L/H and the actual rotational restraint that the orthogonal log-walls and inter-storey floors or roofs can provide, as part of a whole building. As a result, from a practical point of view, it is reasonably expected that k_σ could be approximately assumed between $k_\sigma = 4$ and $k_\sigma = 6.97$ [18], being these values representative of the minimum buckling coefficients for in-plane compressed plates simply supported along the four edges or plates with lateral vertical clamps and simply supports along the top and bottom edges, respectively. Due to the *fully monolithic* assumption of this classical formulation, however, it is also clear that Eq.(7) should represent an 'upper limit' for the expected buckling resistance of the studied log-walls.

In any case, with proper modifications, Eq.(7) could be also applied to log-walls with a single opening, being their load carrying capacity strictly related to the buckling resistance of the $L_{ef}\times H$ portion of wall, where L_{ef} denotes the maximum distance of door openings from the lateral supports (Fig.5). For a plate with three edges simply supported and one vertical edge free, Eq.(7) could in fact estimate the expected critical load $N_{cr,0}^{(E)}$ by taking $L \equiv L_{ef}$ and $k_\sigma = 1.277$ [18].

3.3. Column buckling

Final assessment of the buckling strength of *Blockhaus* walls under in-plane vertical compression could be provided by classical analytical formulations of axially compressed, monolithic columns [18]. In the case of log-walls with double door and window openings, in fact, it is expected that their global buckling resistance could depend on the strength contribution of their $b\times L_i\times H_d$ resisting portion (Fig.2a), and that the corresponding critical load could be reasonably estimated as:

$$N_{cr,0}^{(E)} = \frac{\pi^2 E I_{ef}}{\overline{H}^2}, \quad (8)$$

with

$$I_{ef} = \frac{b^3 L_i}{12} \quad (9)$$

the flexural moment of inertia, $E \equiv E_\perp$ and

$$\overline{H} = \beta H_d \quad (10)$$

the effective buckling length.

In Eq.(10), H_d represents the maximum height of openings, while β is the buckling coefficient accounting for the actual restraint condition. Since the $b \times L_i \times H_d$ portion is part of a more structured geometry (Fig. 2), β is set in this study equal to 0.7 as for a clamped-pinned column [19].

Also under these circumstances, it is clear that the column buckling approach is not able to describe the interlocking mechanism between overlapping timber logs, being the estimated Euler's critical load (Eq.(8)) referred to a monolithic column with full isotropic behaviour. Conversely, compared to Eq.(4), the same approach accounts for the RTL (Restrained Top Log, see Fig.9) boundary condition provided by inter-storey floors, hence leading to an appreciable increase of the overall buckling resistance.

4. Finite-element numerical models

In order to investigate the accuracy of the analytical formulations presented in Section 3, as well as to perform a parametric study on a wide series of possible geometrical configurations, detailed Finite-Element (FE) models were implemented in a widespread software package such as ABAQUS/Standard [14].

4.1. General numerical approach

The typical Finite-Element (FE) model used in this investigation consisted of 8-node, linear brick, solid elements with reduced integration (C3D8R), available in the ABAQUS element library

According to the test setup discussed in [4,5], in each simulation a single wall laterally restrained by two orthogonal walls working as outriggers was firstly analysed (Fig.6a). Based on earlier works [3], each timber log was described with a regular $b \times h$ cross section. While the characteristic small protrusions and tongues along the top and bottom surfaces were reasonably neglected (Fig.3a), however, the nominal geometry of logs near the end restraints was correctly reproduced (Fig.6).

At the same time, suitable surface contact algorithms were implemented to properly describe the mechanical interaction between logs composing the main tested walls, as well as between the logs of outriggers and their reciprocal contact surfaces. Possible tangential sliding was allowed between the logs (*tangential behaviour*), with $\mu = 0.5$ being the static friction coefficient [3]. The detachment of logs in the direction perpendicular to the contact surfaces was also taken into account (*normal behaviour*), so that the influence of partial uplift and overturning of logs on the overall bending deformations of the examined log-walls could be investigated.

Concerning the mechanical characterization of timber, C24 spruce was preliminary defined as an indefinitely linear elastic, isotropic material having density $\rho = 420 kg/m^3$, nominal average MOE $E \equiv E_{\perp} = 370 MPa$ and shear modulus $G = 500 MPa$ [6]. At the same time, possible compressive damage and local failure mechanisms occurring in the timber logs (e.g. localized crushing mechanisms along protrusions and grooves of main logs) were preliminary neglected, being estimated of minor effect on the global buckling resistance of the studied log-walls. In accordance with the buckling test setup described in [4][5], each main wall was then subjected to a concentrated mid-span compressive load N. No restraints were introduced at the top log

of the main walls (UTL, Unrestrained Top Log, hypothesis), while boundaries were defined at their base log only (u_x= 0, u_y= 0, u_z= 0; Fig.6a).

4.2. Preliminary validation of FE-models on past experiments and analytical formulations

4.2.1. Eigenvalue buckling analyses *(eb)*

Validation of the numerical modelling assumptions discussed in Section 4.1 was preliminarily carried out against the critical buckling loads obtained by Heimeshoff and Kneidl on both the (1:4) and (1:1.4)-scaled specimens depicted in Fig.2.

Firstly, eigenvalue buckling analyses (denoted with *eb* in the following) were performed on various FE-models, in order to compare the obtained critical load predictions with the corresponding experimental results [4][5] and with the analytical formulations mentioned in Section 3 (with $E_{||}$=1100MPa, $E_{\perp}$= 370MPa, G= 500MPa the elastic moduli of spruce [4, 5]). Results are summarized in Table 1 for specimens without openings, with a single door opening or with double door/window openings.

Compared to UTL analytical predictions (Eqs.(2)-(4)), experimental critical loads obtained for log-walls with or without openings generally resulted markedly higher than expected. A mean percentage ratio $\Delta_{mean}\approx$ -52% – being $\Delta = 100 \cdot \left(N_{cr}^{analytical} - N_{cr}^{avg.test} \right) / N_{cr}^{avg.test}$ – was in fact found between average test results and corresponding analytical predictions listed in Table 1, with discrepancies generally increasing with the number of openings ($\Delta\approx$ -39%, $\approx$ -56% and$\approx$ -67% for specimens without openings, with single door opening or double openings respectively). Numerical *eb* results provided by geometrically refined FE-models (Fig.7a), otherwise, typically highlighted appreciable agreement between buckling test failure loads and eigenvalue predictions ($\Delta_{mean}\approx$ -13%, with $\Delta \approx$ +2%, $\approx$ -21% and $\approx$ -22% for specimens without openings, with single or double openings respectively).

In a second modelling phase, based on comparative buckling analyses presented in Table 1, geometrical simplifications were also implemented in the same FE-models, and their computational efficiency was improved by replacing the lateral outriggers and their related surface-to-surface interactions, with equivalent boundary conditions (Fig. 6b). Vertical rollers able to prevent possible out-of-plane and in-plane horizontal displacements of the main log-walls (u_x= 0 and u_z=0) were introduced where the contact between main logs and the outriggers occurs (Fig. 6b and detail). This modelling assumption resulted in distributed nodal boundaries generally able to reproduce well the typical restraint offered by corner joints and orthogonal log-walls. Due to the well-defined surface of application of rollers, the same modelling assumption also showed an appreciable restraint of main logs against r_y rotations, hence suggesting the presence of clamps rather than simply supports along the vertical edges of specimens. Agreement between *eb* predictions obtained from FE-models with outriggers and with equivalent boundaries was considered satisfactory and typically resulted, as shown in Table 1, in negligible discrepancies ($\approx$ +1.2%) and coincident overall buckling deformed shapes for the examined log-walls (e.g. Fig. 7), hence suggesting the possibility to use the computationally more efficient second type of FE-models for further parametric studies.

4.2.2. Static incremental buckling analyses *(sib)*

Incremental buckling (*sib*) analyses were then performed, in order to compare the few available load-displacement test measurements discussed in [4, 5] with the corresponding numerical predictions. Critical buckling loads contain only partial information on the buckling behaviour of a given structural system. Incremental buckling analyses, in this sense, should be preferred in order to investigate its progressive buckling behaviour up to failure, as well as to highlight the effects of several mechanical and geometrical variables such as initial curvatures, load eccentricities, material defects, etc., on its load carrying capacity.

The typical (*sib*) simulation, specifically, consisted in a static step characterized by a monotonic, linear increase of the assigned compressive mid-span load *N*. An initial imperfection set as initial out-of-plane curvature u_0 was implemented in this case. Boundaries (UTL condition), surface-to-surface interactions and mechanical properties of C24 spruce were described as shown in Section 4.2.1 for the geometrically simplified FE-models (Fig. 6b).

Fig.8 displays the load *N*-transversal displacement *u* monitored at the control point P3 (Fig.3a) for one of the B02 specimens. As shown, during the experiment, the log-wall was loaded up to the expected critical buckling load (Eq.(3)), then unloaded to ≈20% of the same value, and finally reloaded up to failure.

The experimental load-displacement plot is compared in Fig. 8a to numerical ABAQUS *sib* predictions, as well as to critical loads obtained from the B02 series of experiments (average value of three specimens) and the corresponding *eb* ABAQUS prediction (UTL). The performed (*sib*) simulation showed good agreement with the corresponding (*eb*) analysis, being the critical load $N_{cr,0}^{(E)}$ obtained from the *eb* simulation representative of the asymptotical value for the expected buckling resistance. Compared to experimental *N*-*u* results, the FE-model showed satisfactory correlation in terms of overall buckling response for the examined log-wall, providing accurate predictions in the first loading phase (e.g. for compressive loads *N* up to ≈50kN) but partial overestimation of the expected resistance and stiffness for higher loads. Optimal agreement was also found between ABAQUS *eb*-*sib* buckling failure loads and the average critical load obtained for the B02 series of specimens. *Sib* simulation, as proposed in Fig. 8b, also emphasized the occurrence of a buckling failure mechanism characterized by partial uplift and overturning of few top logs, with collapse due to progressive detachment of some log-wall components.

Although appreciable agreement was found between experimental, numerical and analytical estimations collected in Fig.8a, it should be noticed that the mentioned results were strictly related to the examined loading (e.g. mid-span concentrated load *N*) and boundary (e.g. UTL) conditions. The presence of in-plane rigid inter-storey floors (RTL condition), for example, would result in markedly different overall behaviour for the examined log-wall specimens, as well as in higher buckling resistances. Examples are proposed in Fig. 9, where the fundamental modal shapes obtained for some FE-models derived from specimens of [4,5] are shown (ABAQUS-RTL *eb*). In them, additional restraints were introduced along the top edge of each log-wall, in order to prevent possible transversal displacements due to the applied mid-span compressive loads *N* (u_x= 0). Compared to critical loads listed in Table 1, *eb*-RTL simulations generally resulted in

Euler's buckling loads up to ≈3 -4 times higher for the same log-walls, depending on their geometry and number of openings (e.g. $N_{cr,0}^{(E)} \approx 237$kN for B02 type specimens). Simulations also highlighted, as expected, that the presence of in-plane compressive, distributed pressures *q* rather than mid-span compressive forces *N*, would lead to a more realistic loading condition for the examined log-walls, but also to further increase (up to ≈ 1.3 times) of the buckling resistances of the same specimens. Further extended investigations are consequently required.

4.3. Further assessment of FE-models

Based on assessment of FE-models applied to past experiments [4, 5] proposed in Section 4.2, parametric numerical studies were then carried out to further investigate the effects of the main influencing parameters on the predicted buckling response of timber log-walls. To save space, exemplificative comparisons obtained from various FE-models are proposed in the following sections only for the case of *L*= 4m × *H*= 2.945m 'Tirol' log-walls without openings.

4.3.1. Top boundary condition

The actual restraint provided by inter-storey floors generally adopted in *Blockhaus* structural systems was firstly assessed. In *Blockhaus* buildings, the typical inter-storey floor consists in fact of a series of timber joists connected to the supporting walls by means of notches able to provide appropriate interlocking between them (Fig.10a). *Eb* analyses, in this sense, were performed in ABAQUS/Standard on FE-models able to reproduce the effective geometry of a typical floor (Fig.10b) and its connection to the supporting log-walls. A uniformly distributed pressure *q* was then applied to the top surface of this inter-storey floor.

Eb simulations confirmed their diaphragm effect on the global behaviour of the main log-walls. The fundamental buckling shape displayed in Fig.10c, for example, refers to a *Blockhaus* structural system having square base shape (*L*= 4m) and height *H*=2.945m. The log-walls are obtained by assembling a series of 'Tirol' timber logs (Fig.1b). In accordance with the standard [19], hypothesizing the FE-model of Fig.10 as representative of a residential building, the inter-storey floor that is able to resist gravity loads was assumed as a series of timber joists with cross-sectional dimensions b_{joist}=120mm ×h_{joist}=230mm (Fig. 10a), spaced at *i*= 0.75m and supporting a rigidly connected 32mm-thick OSB flooring panel. As shown in Fig.10c, a fundamental modal shape in good agreement with preliminary RTL deformed shapes of single log-walls (e.g. Fig.9a) was obtained, hence suggesting the correctness of the RTL restraint assumption for further extended investigations.

4.3.2. Local damage of logs for compression perpendicular to the grain

The possibility of local damage mechanisms of logs due to compression perpendicular to the grain was also numerically investigated. The indefinitely linear elastic mechanical behaviour of C24 spruce adopted in the preliminary FE-models discussed in Section 3 was replaced with an idealized elasto-plastic curve, being $E_{\perp}$=

370MPa the average MOE and $f_{c,90} \approx f_{c,90,k} / 0.7 \approx 3.57$MPa the mean compressive strength perpendicular to the grain, with $f_{c,90,k}$= 2.5MPa signifying the corresponding nominal characteristic value [15].

Sib simulations highlighted that possible plasticization in compression typically occurs at the centre of log-walls (e.g. where the log-walls attain the maximum out-of-plane displacements, in accordance with the modal shapes proposed in Fig.9 or Fig.11) and these phenomena are limited to small portions of their total width *L*. Compared to *sib* predictions obtained with full linear elastic FE-models, the effect of timber plasticization in compression generally manifested in about 2-5% difference, in terms of maximum buckling load N_{max} for a same log-wall (Fig.11).

In any case, since the use of indefinitely linear elastic material would result in non conservative estimations, the assumption of an elasto-plastic mechanical model was preferred and used in the analyses performed in the following.

4.3.3. Initial imperfections and load eccentricities

Despite the negligible dependency of *sib* numerical predictions on compressive local damages, the buckling resistance of the studied log-walls was markedly dependent on the amplitude of initial geometrical out-of-plane curvatures u_0. In this sense, while lack of straightness in single timber logs is generally ensured by requirements of production standards (e.g. a maximum deviation from straightness of ≈1-1.5mm/m is allowed for beam-like structural elements composed of timber (e.g. [20])), global imperfections and curvatures deriving from assembly and installation on site of log-walls structures, as well as possible defects in timber or corner joints, should be properly taken into account for design purposes. *Sib* buckling analyses were in fact performed on FE-models of log-walls affected by preliminary overall curvatures described in the form of scaled fundamental modal shapes (RTL condition) obtained from (*eb*) simulations. The maximum amplitude u_0 of these buckling shapes, specifically, was scaled to well-defined ratios ($0 \leq u_0/H \leq 0.005$), so that the obtained deformed configurations could be used in *sib* analyses for the application of the incremental compressive loads *N*.

Parametric simulations highlighted that the presence of these imperfections – although strictly depending on the maximum amplitude u_0/H – can decrease the ideal Euler's critical load $N_{cr,0}^{(E)}$ of a geometrically flat log-wall up to 30-40%. This effect mainly derives from premature detachment, uplift and overturning of few overlapping logs, typically located where maximum out-of-plane displacements are expected (e.g. at the centre of the log-wall, Fig. 11b) and resulting in a marked loss of load carrying capacity. Plots displayed in Fig.11a refer to a 'Tirol' log-wall with overall dimensions *L*=4m×*H*= 2.945m and no openings. Load *N*-displacement *u* results, with *u* signifying the maximum envelope of out-of-plane deflections, refer to the same log-wall affected by initial imperfections of various amplitudes. The same curves are compared with the Euler's critical loads estimated by means of Eq.(7). The difference among the three asymptotical Euler's loads $N_{cr,0}^{(E)}$ displayed in Fig.11a is given by the type of boundary condition considered, namely by assuming in Eq.(7) a buckling coefficient k_σ equal to: (i) 4 (*ss-ss*, corresponding to a plate with all edges simply

supported); (ii) 6.97 (*cc-ss*, corresponding to a plate with lateral clamps and top-bottom simply supports); and (iii) 8.83 (*cc-cc*, corresponding to a plate with all edges clamped). As shown, the gradual increase of the u_0/H ratio clearly leads to a significant decrease of both initial stiffness and maximum load N_{max}. While for the log-wall with null initial curvatures the predicted buckling resistance N_{max} could be reasonably estimated by Eq.(7) with k_σ= 6.97, Fig.11a highlights that both the *ss-ss* and *cc-cc* would not provide appropriate estimation for $N_{cr,0}^{(E)}$, since respectively underestimating and overestimating the actual restraints available along the log-wall edges. Based on recommendations provided by Eurocode 5 [19], in any case, a minimum initial curvature of amplitude $u_{0,min}$= 0.0025H corresponding to an intermediate value of dimensional tolerance recommended for glue-laminated members ($u_{0,min}$= 0.002H) and solid wood members respectively ($u_{0,min}$= 0.0033H) could be taken into account for stability check purposes.

Concerning possible load eccentricities e_{load}, appropriate numerical investigations were also performed. While the typical connection between inter-storey floors and main walls in *Blockhaus* buildings is in fact realized as depicted in Fig.10, in some circumstances – due to mainly architectural demands or technical requirements (e.g. presence of adjacent buildings) – the floor joists are interrupted within the thickness b of the supporting walls (e.g. Fig.12). Proper connection between each joist and the main logs is then ensured by steel screws, e.g. with length l_{screw}= 220mm and diameter ϕ_{screw}= 8mm (detail of Fig.12). *Sib* simulations performed on log-walls eccentrically loaded typically resulted in further decrease of initial stiffness and corresponding ultimate load N_{max}, compared to the same log-walls affected by initial curvatures only. An example is displayed in Fig.11a for the 'Tirol' specimen (L=4.5m×H= 2.945m), with combined curvature (u_0/H= 0.0025) and a given load eccentricity ($e_{load}\approx b/4$). As shown, compared to the same log-wall with initial imperfections only (u_0/H= 0.0025), the additional load eccentricity leads to a further ≈20% decrease of buckling resistance, hence resulting in and overall ≈30% decrease of the load carrying capacity estimated for the geometrically flat and axially compressed log-wall.

4.3.4. Geometrical description of logs

FE-models able to reproduce the nominal profile of logs were also developed (e.g. Fig.1), and compared to log-walls with regular b×h cross-sections. *Sib* simulations generally resulted in partial – often negligible – improvement of interlocking between logs offered by small protrusions and tongues along the contact surfaces, and consequently in almost identical stiffness, overall deformed shape and ultimate buckling resistance N_{max} for these FE-models (Fig.13). The implementation of protrusions and tongues – typically requiring further mesh refinement and increased computational cost of analyses – was consequently avoided.

4.3.5. Validation of FE-models to full-scale experiments

Prior to the execution of parametric studies on log-walls with various geometrical properties, final validation of FE-numerical models was developed by taking into account test predictions obtained by full-scale buckling experiments recently performed at the Laboratory of Structural Engineering of the University of

Trieste (Italy), Department of Engineering and Architecture. Experiments were performed in non-controlled laboratory conditions, during June and July 2014, and the typical duration of buckling tests resulted in the range of 8-10 minutes.

Careful consideration was given in this work to analyse configurations currently produced by Rubner Haus [16]. Buckling experiments, accordingly, were performed on log-wall specimens composed of 'Tirol' logs, having overall dimensions L= 4m × H= 2.945m and characterized by the presence or not of double door and window openings. In doing so, an appropriate experimental setup was developed, in order to provide the desired loading and boundary conditions to the tested walls (Fig.14). As result, the typical full-scale specimen was positioned on the strong floor and laterally restrained at the top log by means of additional metal bracings, so that the desired RTL condition could be properly reproduced (detail of Fig.14c). Specimens were tested by taking into account also a desired loading eccentricity e_{load}. To reproduce the effect of distributed loads deriving from inter-storey floors or roofs, quasi-static monotonic compressive loads N were applied by means of five hydraulic jacks equally spaced along the specimen width L, and gradually increased up to failure (Fig.14b). The applied compressive loads were monitored by means of a load cell, while out-of-plane and in-plane deformations of specimens were monitored during each test by means of 10 + 4 transducers with a resolution of 0.01mm (Fig. 14a).

Specimen LW01, consisting of a 'Tirol' log-wall without openings and an assigned load eccentricity e_{load}= b/2, failed at the attainment of a maximum compressive load N_{max}= 233.2kN. As expected, the wall manifested up to failure a typical 'plate buckling' deformed shape of an almost fully monolithic plate pinned at the top and bottom edges and clamped along the lateral edges, due to the adopted 'Standard' corner joints. As result – although partly affected by the applied load eccentricity e_{load} – the obtained deformed shape was characterized by maximum out-of-plane displacements located at the centre of the specimen (control point P06, Fig.14a), but almost null transversal displacements at the top log, due to the adopted test setup (Fig.14c). Collapse of the wall occurred due to partial cracking and progressive detachment of its four top logs which buckled out-of-plane together with the four logs immediately below, while no damage was generally noticed in the 'Standard' corner joints. Concerning the protrusions and tongues characterizing the typical 'Tirol' profile, due to the flexural deformed shape attained in the log-wall near collapse, minor damages were found only at the external ends of the four top main logs. An overview of the obtained deformed shape is provided in Fig.15a, together with the corresponding FE prediction (Fig.15b). Experimental results are also proposed in Fig.15c in the form of load N vs. the ratio between maximum out-of-plane deformations u (max. envelope of control points P01-P10, Fig. 14a) and the specimen height H. As shown in Fig.15c, after attaining its maximum load carrying capacity at point A (N_{max}≈ 237kN), the specimen was unloaded due to lack of residual resistance deriving from overturning of its top logs. The FE-model of specimen LW01 was implemented as discussed in previous sections (e.g. Fig.6b) and timber, accordingly, was described by taking into account the average MOE $E_{\perp}$, the mean longitudinal shear modulus G and the average compressive strength perpendicular to the grain $f_{c,90}$ experimentally measured from additional small

timber specimens. As shown in Fig.15, the FE-model provided optimal agreement with test measurements, hence justifying all the modelling assumptions (e.g. simplified rectangular $b \times h$ profile of logs; equivalent isotropic, elasto-plastic mechanical behaviour for spruce; equivalent lateral restraints along the vertical edges of the log-wall).

Further validation of the same FE-modelling approach is proposed in Fig.16 for the specimen LW02, having the overall dimensions of specimen LW01, but characterized by the presence of door and window openings (L_i= 1.18m), as well as by a smaller load eccentricity $e_{load} \approx b/5$. The main feature of *Blockhaus* log-walls with openings produced by Rubner Haus is that 3mm-thick, hollow section steel profiles with nominal dimensions 25mm×40mm are usually introduced along the vertical edges of openings, in order to improve the interaction between the adjacent timber logs and to increase the global flexural stiffness of the studied structural systems (Fig.17). Accordingly, the FE-model of specimen LW02 was properly modified and steel profiles were implemented in it. Steel was described in the form of an isotropic material with an elasto-plastic behaviour (with E_{steel}= 200GPa, ν_{steel}= 0.3 and $f_{y,steel}$= 275MPa the MOE, Poisson's ration and yielding strength respectively). Additional mechanical interactions were introduced between the steel profiles and the timber logs, along their respective contact surfaces. Based on observation of test results obtained for the specimen LW02, as well as on preliminary numerical studies not included in this work, a rigid interaction able to avoid relative displacements along the contact surfaces was assumed between them. As shown in Fig. 16, the experiment on specimen LW02 confirmed the expected 'column buckling' behaviour of the portion of wall comprised between the openings (Fig.16a). Due to metal stiffeners – able to provide large ductility and strengthening contribution to the specimen although by means of contact interactions only – the log-wall LW02 manifested a stable overall buckling behaviour up to failure. Good agreement was found again with the corresponding FE-model (ABAQUS *sib*, Fig.16b).

5. Extended numerical parametric study on log-walls with various geometrical configurations

Based on validation of FE-models to past experiments and further full-scale buckling tests, a wide series of numerical eigenvalue (*eb*) and static incremental (*sib*) buckling analyses were successively performed on various log-walls characterized by different number and position of door and window openings, overall dimensions $L \times H$ and cross-sectional dimensions $b \times h$ (e.g. 'Tirol' and 'Schweiz' log profiles of Fig.1). All the numerical simulations, according to Section 4, were carried out on FE-models with equivalent boundary conditions depicted in Fig.6b, subjected to distributed compressive loads and with the RTL boundary condition. An equivalent isotropic, elasto-plastic mechanical behaviour for C24 spruce was assumed.

Numerical and analytical comparative calculations are assessed and discussed separately for each wall configuration in Sections 5.1 to 5.3.

5.1. Log-walls without openings

Calculations performed on 'Tirol' and 'Schweiz' log-walls generally highlighted a rather good agreement between *eb* numerical and analytical Euler's critical loads provided by Eq.(7), with k_σ= 6.97 the buckling coefficient assumed as for a laterally clamped plate simply supported at the top and bottom edges. Comparative calculations are listed in Table 2 for log-walls without openings. Labels provided for the presented FE-models are representative of the number of openings ("W0"), the breadth of logs ("0.08" and "0.12", in meters, for 'Tirol' and 'Schweiz' profiles respectively), as well as the overall wall length *L*, varied in the 3.5m to 6m range in this exploratory investigations. In the same Table, *eb* predictions are firstly compared to analytical critical loads $N_{cr,0}^{(E)}$ given by Eq.(7). Based on Fig.11a, the difference among the four analytical predictions for each log-wall geometry is given by the reference boundary condition taken into account ('*ss-ss*': all simply supported edges; '*cc-ss*': lateral clamps and top-bottom simply supports), as well as the accuracy in the estimation of the corresponding buckling coefficient ($^{(i)}$: k_σ= *f(H/L)* or $^{(ii)}$: $k_\sigma = k_{\sigma,min}$ for the specific boundary condition).

As expected, assumption of simply supports along the lateral edges (*ss-ss*) would strongly underestimate the expected critical load $N_{cr,0}^{(E)}$ for the examined log-walls, both by using the approximate estimation of k_σ ($k_{\sigma,min}$ - avg. $\Delta_2 \approx$ 72%) and the more refined buckling coefficient k_σ= *f(H/L)* (avg. $\Delta_1 \approx$ 41%). Accounting for lateral clamps along the vertical edges to represent the actual restraint provided by corner joints (*cc-ss*), otherwise, would provide an appropriate prediction of the expected critical load $N_{cr,0}^{(E)}$ (avg. $\Delta_3 \approx$ -4.1%), hence suggesting the use of k_σ = 6.97 in Eq.(7) for practical calculations. In terms of ultimate buckling resistance N_{max} obtained for the same log-walls from (*sib*) simulations, moreover, the presence of initial curvatures typically resulted in marked reduction of the corresponding critical load $N_{cr,0}^{(E)}$. Comparisons are proposed in Table 2 for log-walls affected by an initial geometrical imperfection with maximum amplitude u_0/H= 0.0025. As shown, a different average discrepancy Δ_5 was found for 'Tirol' (≈37%) and 'Schweiz' (≈51%) log-walls, due to sensitivity of the examined log-wall type and buckling behaviour to the cross-sectional ratio of profiles, to their overall aspect ratio *L*/*H* as well as to the combination of these parameters with the amplitude of initial curvatures or possible compressive localized damages in timber (e.g. short 'Schweiz' log-walls are less susceptible than 'Tirol' log-walls to out-of-plane deformations). As result, comparisons shown in Table 2 confirmed the importance of a simplified design method able to take into account the effects of imperfections.

5.2. Log-walls with single door opening

Log-walls with single door opening were investigated next. Numerical and analytical results obtained for *Blockhaus* walls with total length *L* ranging between 3.5m and 6m and single door opening (L_d= 1.23m, H_d= 2.23m) differently spaced from the lateral restraints (e.g. Fig.5, L_{ef}) are compared in Table 3. The differences

among the labels of the FE-models with single door opening ("W1") displayed in Table 3 are given by the overall length L of the same log-walls (in meters), as well as by the maximum distance of openings from the lateral edges (e.g. L_{ef}, in meters). All these FE-models refer to the case of 'Tirol' logs. Like for the log-walls without openings, *eb* analyses were firstly performed to assess the strengthening contribution of metal profiles introduced – in Rubner Haus current practice – along the vertical edges of doors (Fig.17).

Simulations highlighted, for the investigated geometrical configurations, that these steel profiles apparently provide a moderate increase of the expected critical load $N_{cr,0}^{(E)}$, compared to log-walls with the same nominal geometry but without the metal stiffeners (avg. $\Delta_1 \approx 5.8\%$, Table 3). Fundamental modal shapes comparable to Fig.9b were generally found for the examined log-walls, hence confirming that their load-carrying capacity is almost fully governed by the $L_{ef} \times H$ portion comprised between the opening and one of the lateral end restraints.

Otherwise, analytical predictions obtained for the same critical loads $N_{cr,0}^{(E)}$ generally provided conservative estimations, with an average discrepancy from the corresponding *eb* values equal to $\Delta_2 \approx 48.7\%$. This difference, as confirmed by further analysis of results displayed in Table 3, can be justified both by the assumption in Eq.(7) of a constant buckling coefficient $k_\sigma = 1.277$ for all the investigated log-walls, and by the absence in the same equation of an additional term accounting for the strengthening and stiffening contribution of metal profiles. The use of $k_\sigma = 1.277$ in Eq.(7), consequently, would markedly underestimate the effective theoretical critical load $N_{cr,0}^{(E)}$, but could be taken into account for a practical, simplified and conservative design approach. As expected, finally, implementation in the same FE-models of initial curvatures agreeing with Fig.9b and having a maximum amplitude $u_0/H = 0.0025$, generally resulted in a further marked decrease of the corresponding Euler's critical load, almost stable for all the examined geometrical configurations (Table 3, avg. $\Delta_3 \approx 20\%$).

5.3. Log-walls with double door and window openings

Additional (*sib*) simulations were finally carried out on *Blockhaus* walls characterized by the presence of a double door and window opening with nominal dimensions $L_d = 1.23\text{m} \times H_d = 2.23\text{m}$ and $L_w = 1.23\text{m} \times H_w = 1.33\text{m}$, respectively, spaced at a distance L_i from each other (Fig.2a). Based on results discussed in Sections 5.1 and 5.2, only 'Tirol' log-walls with more slender cross-sections were investigated in this phase. In all these FE-models, independently of the overall geometrical configuration of the examined log-walls, metal profiles were introduced along the vertical edges of openings (e.g. Fig.17).

As expected, (*eb*) and (s*ib*) analyses highlighted that the presence of double openings – especially in conjunction with other geometrical parameters such as initial curvatures u_0 – markedly affects the global buckling response of *Blockhaus* walls under vertical compressive loads. Comparative numerical and analytical results are proposed in Table 4 for log-walls with double openings ("W2"), overall length L (in meters) and a given distance L_i (in meters) between the door and the window. In the same Table, *eb*

predictions are first proposed for the FE-models of the same wall with or without metal profiles. As shown, due to the typical column buckling behaviour highlighted by the investigated FE-models (e.g. Fig.9c), an appreciable benefit was generally found and an average increase in theoretical buckling load of $\Delta_1 \approx 24.8\%$ - depending on the steel stiffeners only - was calculated. Due to this marked strengthening contribution provided by metal profiles, as result, Eq.(9) was modified accordingly, and the improvement in flexural stiffness provided by the adopted steel hollow profiles was accounted for as for a composite timber-steel column (e.g. Fig.17) with total bending stiffness given by:

$$EI_{ef} = E_{\perp}\frac{b^3 L_i}{12} + 2E_{steel}I_{steel}, \tag{11}$$

with I_{steel} the second moment of area of a single metal profile (Fig.17a).

Analytical calculations performed by means of Eq.(8) and Eq.(11) are listed in Table 4 for the examined log-walls. The difference between the analytical values reported in the fifth and seventh column is then given by the value of the effective buckling length $\overline{H}$ considered in the formulas, namely by the specific boundary condition assumed for the $b \times L_i \times \overline{H}$ portion of log-wall. Calculations highlighted that the assumption of a pinned-clamped column (e.g. β=0.7 in Eq.(10)) would in fact partly underestimate the theoretical load carrying capacity of the studied log-wall, providing an average discrepancy $\Delta_2 \approx 48\%$ with respect to the corresponding *eb* values. In any case, the assumption of this boundary condition – although describing in a simplified way the structural interaction between the $b \times L_i \times \overline{H}$ column and the adjacent logs – would provide better agreement than the 'pin-pin' analytical solution (e.g. β=1 in Eq.(10), with avg.(Δ_3)$\approx 203\%$).

Independently of the geometry of log-walls with double openings, moreover, the presence of initial curvatures typically resulted in a large decrease of the expected buckling resistance.

Sib numerical predictions proposed in Table 4, for example, generally show an average decrease $\Delta_4 \approx 57\%$ between theoretical buckling strengths $N_{cr,0}^{(E)}$ and ultimate critical loads N_{max} for the same log-walls, hence requiring the development of properly calibrated design methods. *Sib* analyses also generally confirmed – in full agreement with the LW02 buckling experiment of Fig.16 – that maximum deformations for this log-wall typology mainly occur between the openings (Fig.18), and the ultimate failure load N_{max} is strictly governed by yielding of the central metal stiffener (detail of Fig.18c).

6. Simplified analytical design approach

Final analysis of numerical and analytical results discussed in Section 5 for log-walls with or without openings was performed in order to provide a simplified analytical approach to be used in practice for the stability check of *Blockhaus* timber walls under in-plane compressive loads. In doing so, the design mechanical properties of spruce were taken into account and replaced – both in FE-models and related plate or column buckling equations – the corresponding experimental mean values:

$$E_{\perp,d} = \frac{E_{\perp}}{\gamma_M}, \qquad G_d = \frac{G}{\gamma_M} \qquad f_{c,90,d} = \frac{k_{\mathrm{mod}} f_{c,90,k}}{\gamma_M}, \qquad (12)(13)(14)$$

being $E_{\perp,d}$, G_d and $f_{c,90,d}$ the design MOE in the direction perpendicular to the grain, the longitudinal shear modulus and the design compressive strength perpendicular to the grain, with k_{mod} a coefficient accounting for the duration of load and effect of moisture (k_{mod} = 0.7 for long-term loads and wood protected from direct contact with water [19]) and γ_M =1.3 the partial safety factor of wood, according to the Eurocode 5 [19]. It is in fact expected, based on Eqs.(12)-(14), that the use of design mechanical properties for timber would result in a design buckling resistance markedly lower – at least ≈30%, based on γ_M – than the corresponding mean value.

Under an assigned design load N_{sd}, specifically, the typical *Blockhaus* log-wall should in fact offer a design buckling strength $N_{b,Rd}$ satisfying the condition:

$$N_{b,Rd} = \chi_{imp} \frac{\left(N_{cr,0}^{(E)}\right)_d}{\gamma_1} \geq N_{sd}\,. \qquad (15)$$

According to comparative discussion of numerical and analytical predictions partly proposed in Section 5, it is assumed that the design Euler's critical load $\left(N_{cr,0}^{(E)}\right)_d$ mentioned in Eq.(15), where the subscript "*d*" recalls the use of the design moduli given in Eqs.(12)-(13), could be calculated for log-walls with generic geometrical configurations by means of Eqs.(7) and (8).

For log-walls without openings, it was in fact shown in Sections 4-5 that their overall buckling behaviour is almost comparable to the buckling response of a plate under in-plane compression with lateral clamps and simply supported top-bottom edges. For the sake of simplicity, the buckling coefficient k_σ in Eq.(7) can be assumed equal to k_σ= 6.97 [18]. Careful consideration should indeed be given to timber log-walls with openings. For log-walls with single opening, the design Euler's critical load $\left(N_{cr,0}^{(E)}\right)_d$ could be rationally estimated by means of Eq.(7), by taking into account the buckling resistance of the main L_{ef}×H portion. In this case, the buckling coefficient k_σ could be conservatively assumed equal to k_σ= 1.277 [18]. In presence of log-walls with double door and window openings, otherwise, $\left(N_{cr,0}^{(E)}\right)_d$ should be calculated by means of Eq.(8), being the design equivalent flexural stiffness $\left(EI_{ef}\right)_d$ of their "composite" resisting portion given by Eq.(11), with β= 0.7 in Eq.(10).

In Eq.(15), the coefficient χ_{imp} signifies a buckling reduction coefficient taking into account the effects of initial imperfections such as an initial curvatures u_0/H, loading eccentricities e_{load} or a combination of them. This buckling reduction coefficient χ_{imp} could be estimated as:

$$\chi_{imp} = \left(1 - \frac{e}{b}\right), \qquad (16)$$

with b the width of logs and:

$$e = u_{0,\max} + e_{load}\,, \tag{17}$$

representing the effects of the assigned imperfections (with $u_{0,min}$= 0.0025H the minimum curvature value recommended for design purposes). The application of the χ_{imp} coefficient (Eq.(16)) to the full-scale specimen LW01 discussed in Section 4.3.5, for example, would provide an expected buckling resistance of ≈241kN (Eq.(7) with experimental moduli $E_{\perp,d}$, G_d and k_σ= *f(H/L)*), thus agreeing well with the corresponding experimental failure load N_{max}≈ 237kN (Fig.15). In the case of specimen LW02, otherwise, a conservative failure load ≈148kN – compared to the experimental buckling resistance N_{max}≈ 215kN (Fig.16) – would be obtained by multiplying Eq.(8) for χ_{imp}.

The coefficient γ_1 of Eq.(15), in this context, signifies a buckling safety factor that should account for possible compressive damages of timber and further effects deriving from mechanical interactions between logs, in order to provide appropriate level of safety to analytical methods discussed in Section 5 and a conservative estimation of $N_{b,Rd}$. The coefficient γ_1 accounts for the possible inaccuracy deriving from the use of Eqs.(7) and (8). In Section 5, for example, it was shown that the plate buckling approach applied to log-walls with single door opening would properly describe their expected global buckling behaviour, but would not take into account the positive contribution of metal stiffeners (e.g. Fig.17). For log-walls with double opening, otherwise, the assumption of a pure column buckling mechanism could partly underestimate possible strengthening contributions deriving from the lateral portions of the log-walls. Consequently, it is clear that the coefficient γ_1 should be properly estimated. In this work, calibration of γ_1 was carried out on the base of parametric numerical investigations performed on the log-wall configurations listed in Tables 2, 3, 4. As a result, the value γ_1= 2 is suggested for log-walls without openings or with double door/window openings. For log-walls with single door opening, conversely, the value γ_1= 1 is proposed.

In Fig.19, numerical and analytical design buckling resistances $N_{b,Rd}$ are proposed and compared for log-walls with no, single or double openings. Numerical design strengths, specifically, are calculated by means of ABAQUS *sib* analyses performed on 'Tirol' and 'Schweiz' log-walls affected by an initial curvature u_0/H ($0.001 \le u_0/H \le 0.005$), a load eccentricity e_{load} ($0 \le e_{load} \le b/2$) or a combination of both. In these FE-models, the design mechanical properties of spruce are taken into account, according to Eqs.(12),(13) and (14). Analytical design strengths are calculated for the same log-walls by means of Eq.(15). Also the results obtained from full-scale specimens LW01 (e_{load} = b/2) and LW02 (e_{load} = b/5) and the corresponding analytical predictions are shown in the same Figure. As shown, Eq.(15) with the proposed buckling coefficients χ_{imp} and γ_1 generally provides conservative estimation of design buckling strengths for the examined log-walls, compared to numerical *sib* predictions. Although it is clear that further validation of the proposed design method is required (e.g. full-scale buckling experiments of log-walls with various aspect ratios or log profiles), comparisons and methods discussed in this work could represent a useful background for further extended studies, as well as for the development of simplified design approaches for implementation in codes of practice such the Eurocode 5.

7. Conclusions

In the paper, the buckling behaviour of timber log-walls under in-plane compressive loads was investigated by means of numerical and analytical models. *Blockhaus* structural systems are typically obtained by assembling multiple timber logs. The structural interaction between them is provided by simple contact mechanisms, protrusions and notches able to improve interlocking, being metal connectors often avoided. At the same time, the adopted timber logs have typical slender cross-sectional aspect ratios, hence resulting in structural systems – compared to other traditional structural typologies – susceptible to buckling phenomena.

As shown through finite-element numerical models properly validated on experimental results presented in earlier literature contributions as well as on full-scale buckling tests recently performed, inter-storey floors generally constructed in *Blockhaus* buildings provide a full-restraint to the connected walls. As a result, the positive stiffening contribution of these inter-storey floors should be properly taken into account in calculations.

Otherwise, several mechanical and geometrical variables, such as small initial imperfections, load eccentricities as well as the number, size and position of openings (e.g. doors and windows), could markedly reduce the effective load-carrying capacity of the same structural system. Based on extended parametric numerical simulations, simple analytical formulations were derived from classical theory of plate buckling or column buckling, and applied to log-walls with generic geometrical properties. A simple analytical method developed in accordance with recommendations of Eurocode 5 was then presented and discussed for the buckling design and verification of the studied timber log-walls under in-plane compressive loads.

Although further validation of the presented method could be provided by extended additional studies – e.g. full-scale buckling experiments on log-walls with various aspect ratios – comparisons and findings discussed in this paper represent a background for the development of simplified design approaches and verification methods to be included in future standards and codes of practice.

Acknowledgements

Rubner Haus AG SpA is gratefully acknowledged for the financial and technical support. Dr. Annalisa Battisti is also acknowledged for technical collaboration.

References

[1] Branco J, Araújo JP (2010). Lateral Resistance of Log Timber Walls subjected to Horizontal Loads. Proceedings of the World Conference on Timber Engineering WCTE 2010, Volume 4, pp.2876-2885.

[2] Branco J, Araújo JP (2012). Structural behaviour of log timber walls under lateral in-plane loads. Engineering Structures, 40: 371-382.

[3] Bedon C, Fragiacomo M, Amadio C, Sadoch C (2014). Experimental study and numerical investigation of Blockhaus shear walls subjected to in-plane seismic loads. Journal of Structural Engineering, published online, DOI: 10.1061/(ASCE)ST.1943-541X.0001065.

[4] Heimeshoff B, Kneidl R (1992). Zur Abtragung vertikaler Lasten in Blockwänden – Experimentelle Untersuchungen. Holz als Roh-und Werkstoff 50:173-180.

[5] Heimeshoff B, Kneidl R (1992). Bemessungsverfahren zur Abtragung vertikaler Lasten in Blockwänden. Holz als Roh-und Werkstoff 50: 441-448.

[6] Bouras F, Chaplain M, Nafa Z, Breysse D, Tran H (2012). Experimental behavior of wood columns under extreme loading: cyclic buckling. Proceedings of the World Conference on Timber Engineering WCTE 2012, Volume 5, pp.545-550.

[7] Burdzik WMG, Dekker NW (2012). A rational approach to predicting the buckling length of compression chords in prefabricated timber truss roof structures braced by means of diagonal bracing. Journal of the South African Institution of Civil Engineering, 54(1): 81-89.

[8] Eilering S, Beißner E (2011). Zur Stabilität von BSH-Kreisbogenbindern [On the stability of circular curved beams of glued-laminated timber]. Bauingenieur, 86(2): 76-83.

[9] Baláž I (2005). Lateral torsional buckling of timber beams. Wood Research, 50(1): 51-58.

[10] Mittelstadt C, Brüninghoff H (2002). Biegedrillknicken eines Bogebinders aus Brettschichtholz [Torsional-flexural buckling of an arch-shaped beam made of glued-laminated timber]. Bautechnik, 79(5): 285-296.

[11] Möller G (2004). Ermittlng von Stabilisierungs-Lasten im Holzbau [Calculation of lateral stability loads for timber constructions]. Bautechnik, 81(6): 480-488.

[12] Hofmann R, Kuhlmann U (2010). Influence of creep on the lateral torsional buckling of glued laminated timber girders. Proceedings of 11th World Conference on Timber Engineering WCTE 2010, Volume 1, pp.335-342.

[13] Leicester RH (2009). Buckling strength of timber structures. Australian Journal of Structural Engineering, 9(3); 249-256.

[14] Simulia, 2012. ABAQUS v.6.12 [Computer Software], Dassault Systems, Providence, RI, USA.

[15] EN 338:2009. Structural timber-strength classes. European Committee for Standardization (CEN), Brussels, Belgium.

[16] Rubner Haus AG SpA. www.haus.rubner.com

[17] DIN1052 Teil 1: Holzbauwerke; Berechnung and Ausführung, 1988.

[18] Timoshenko SP, Gere JM (1961). Theory of Elastic Stability, McGraw-Hill, International Book Company.

[19] EN 1995-1-1:2009. Eurocode 5 - Design of timber structures - Part 1-1: General-common rules and rules for buildings. European Committee for Standardization (CEN), Brussels, Belgium.

[20] Ballast DK (2007). Handbook of Construction Tolerances. Wiley & Sons, 2nd Edition.

Figure 1

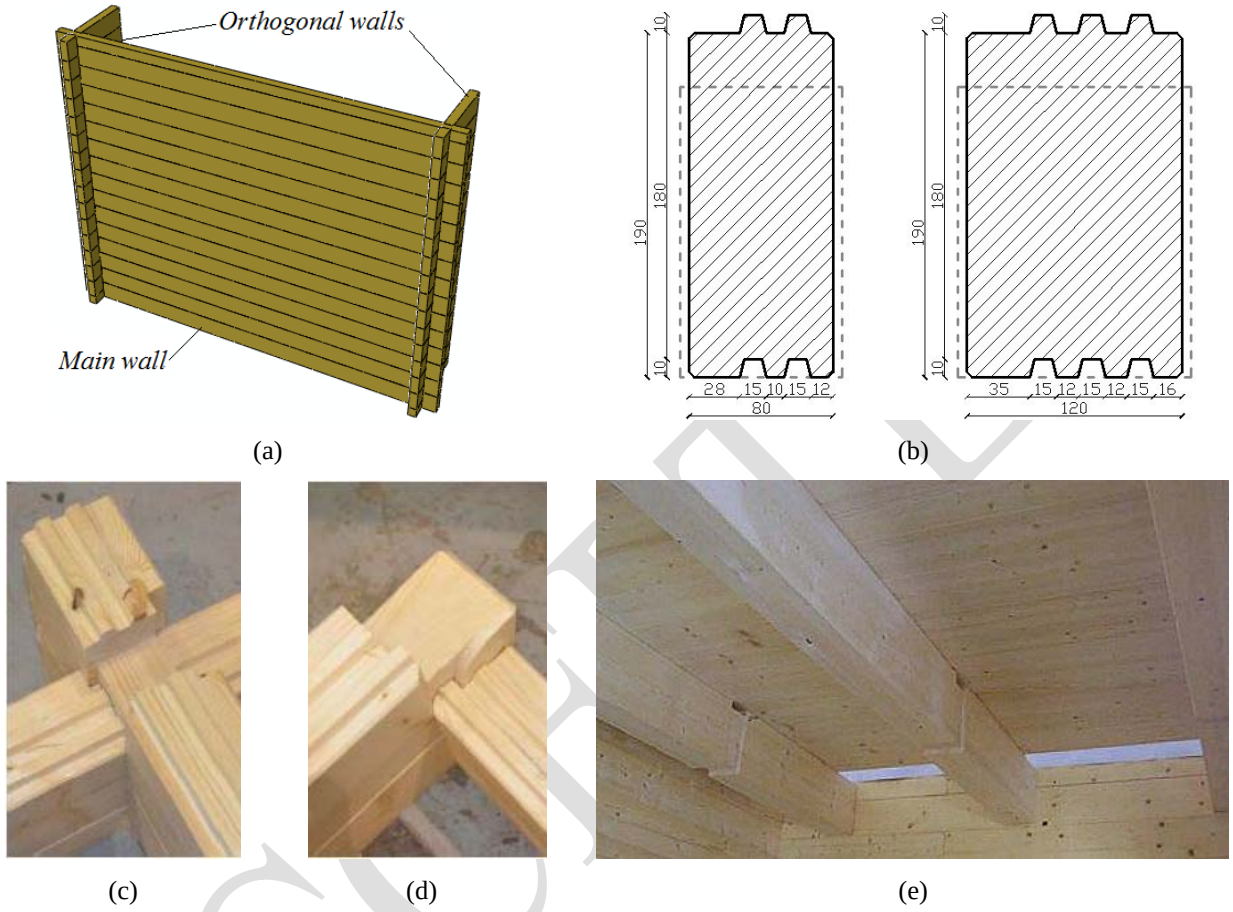

Fig.1. Examples of typical *Blockhaus* structural components. (a) main log-wall; (b) 'Tirol' (left) and 'Schweiz' (right) cross-sections of timber logs produced by Rubner Haus [16] (dimensions in mm; solid and dashed lines denote current and previous manufactured sections, respectively); (c) 'Standard' corner joint; (d) 'Tirolerschloss' corner joint; (e) inter-storey floor.

Figure 2

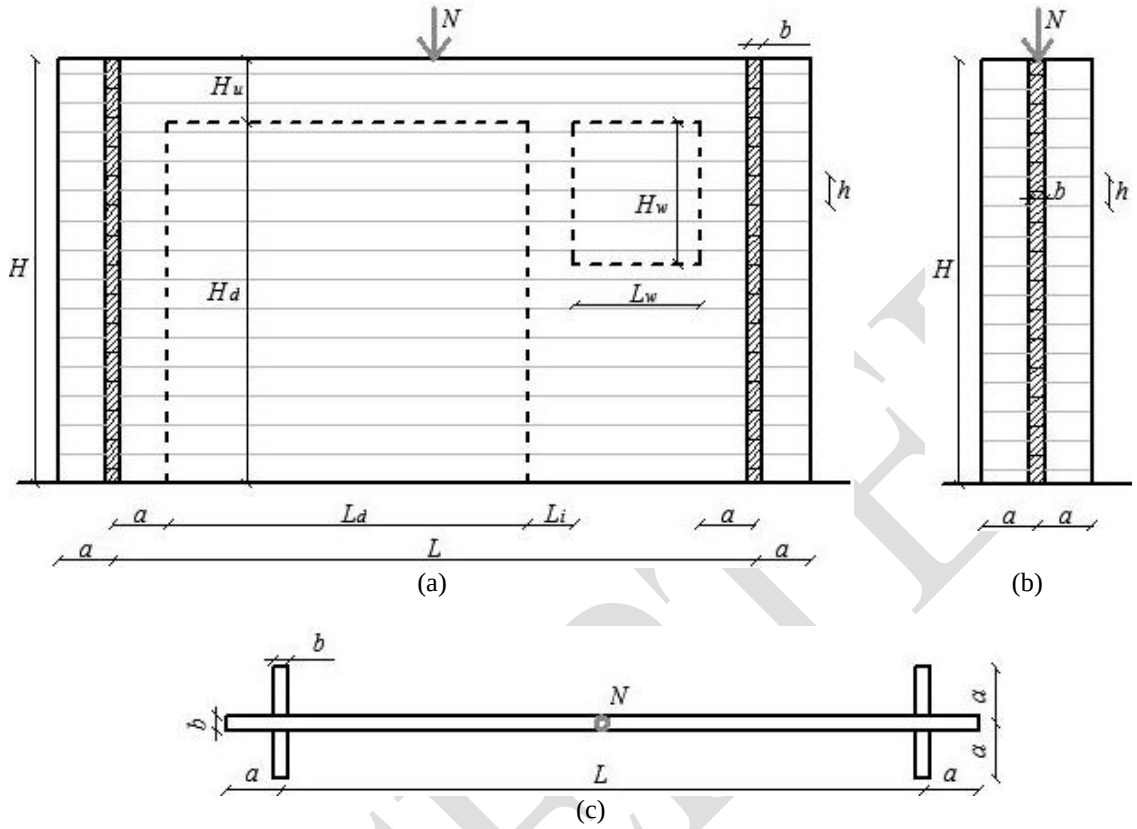

Fig.2. Nominal geometrical properties of series A ((1:4)-scaled) and series B ((1:1.4)-scaled) log-wall specimens tested in [4, 5]. (a) front view; (b) lateral view; (c) top view.

Figure 3

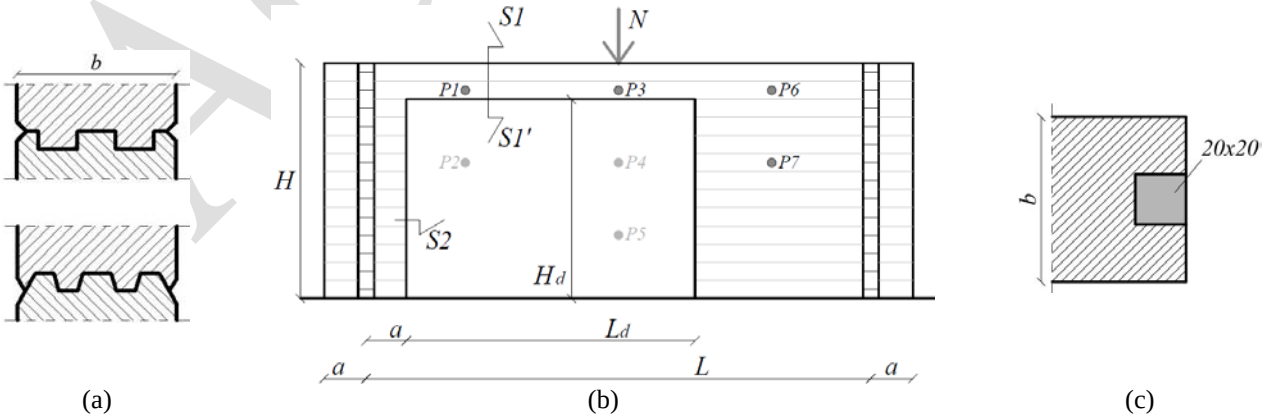

Fig.3. (a) detail of section S1-S1' of timber log profiles adopted in (1:4)-scaled log-wall specimens (series A); (b) position of control points P1-P7 for (1:1.4)-scaled specimens (series B); (c) detail of section S2 for specimens with single door opening and additional metal stiffeners (nominal dimensions in mm) [4, 5].

Figure 4

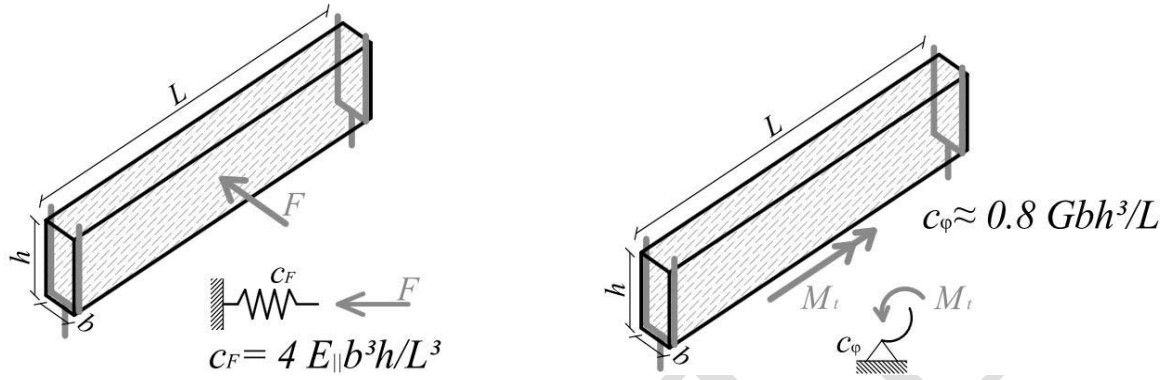

(a) (b)

Fig.4. Analytical model for the calculations of the (a) flexural (c_F) and (b) torsional (c_φ) spring constants [4, 5].

Figure 5

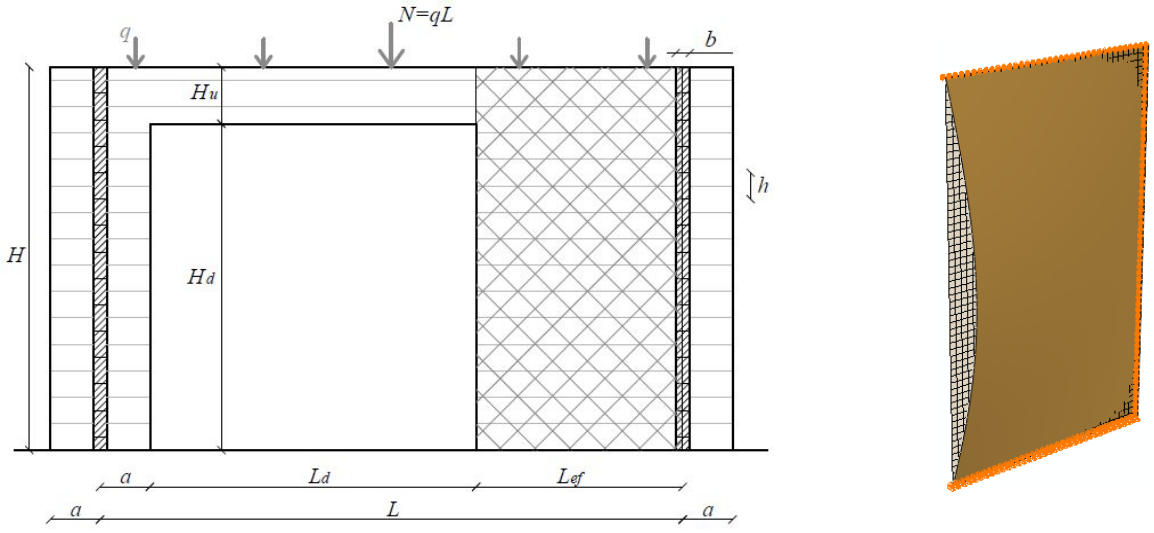

(a) (b)

Fig.6. Log-walls with single door opening. (a) geometry; (b) expected buckling shape of the $L_{ef} \times H$ resisting portion.

Figure 6

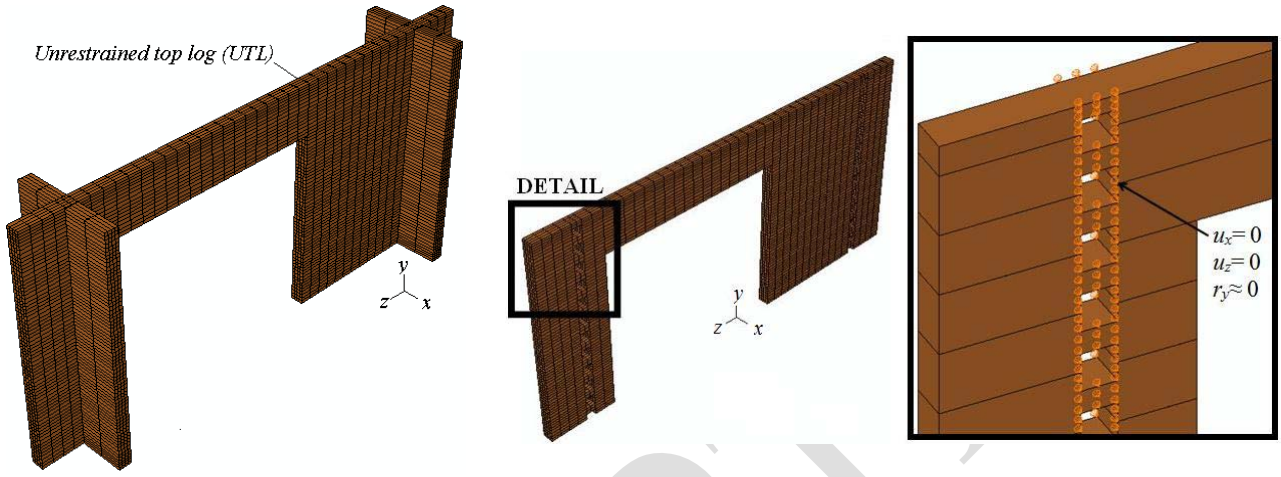

(a) *FE-model with outriggers* (b) *FE-model with equivalent boundaries*

Fig.6. Example of FE-numerical model (ABAQUS).

Figure 7

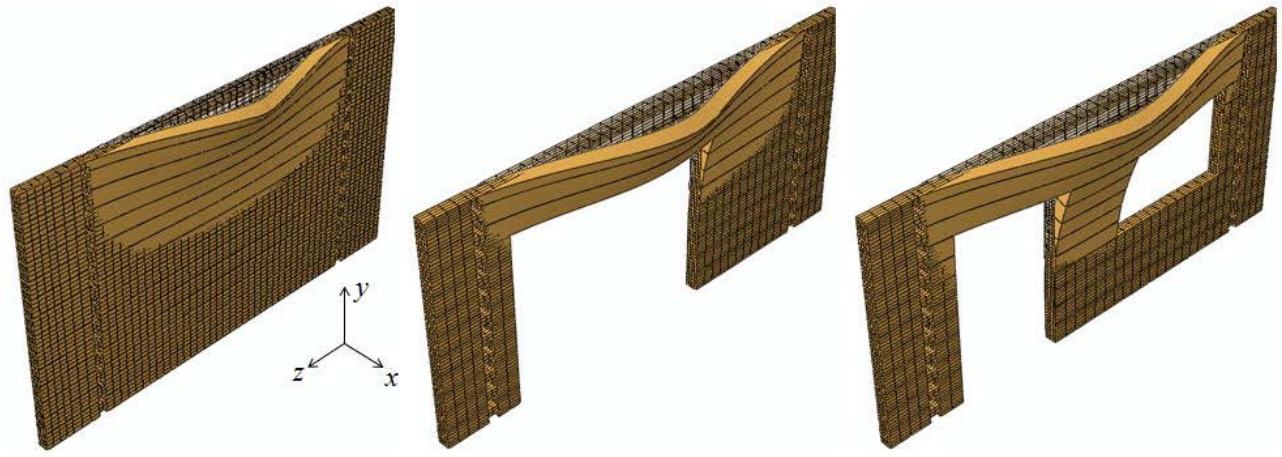

(a) (b) (c)

Fig.7. Fundamental modal shapes obtained from preliminary FE-models (ABAQUS *eb*) for specimens (a) without openings (type A04); (b) with single door opening (type B02) and (c) with double openings (type B04). UTL boundary condition.

Figure 8

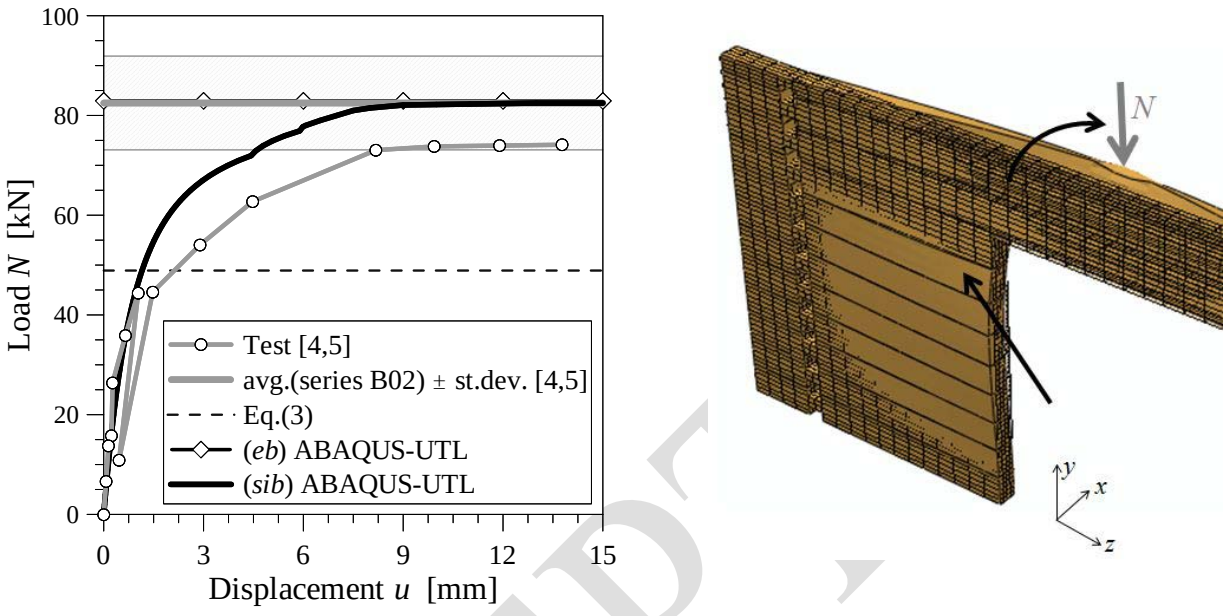

(a) (b)

Fig.8. Buckling analysis on B02 type of specimens. (a) Load *N*-transversal displacement *u* (point of measure P3, Fig.3b). Comparison between test results [4, 5], analytical estimations (Eq.(3)) and numerical predictions (ABAQUS-UTL, *sib* and *eb*). (b) deformed shape, with evidence of progressive detachment and uplift/overturning of logs (ABAQUS-UTL *sib*).

Figure 9

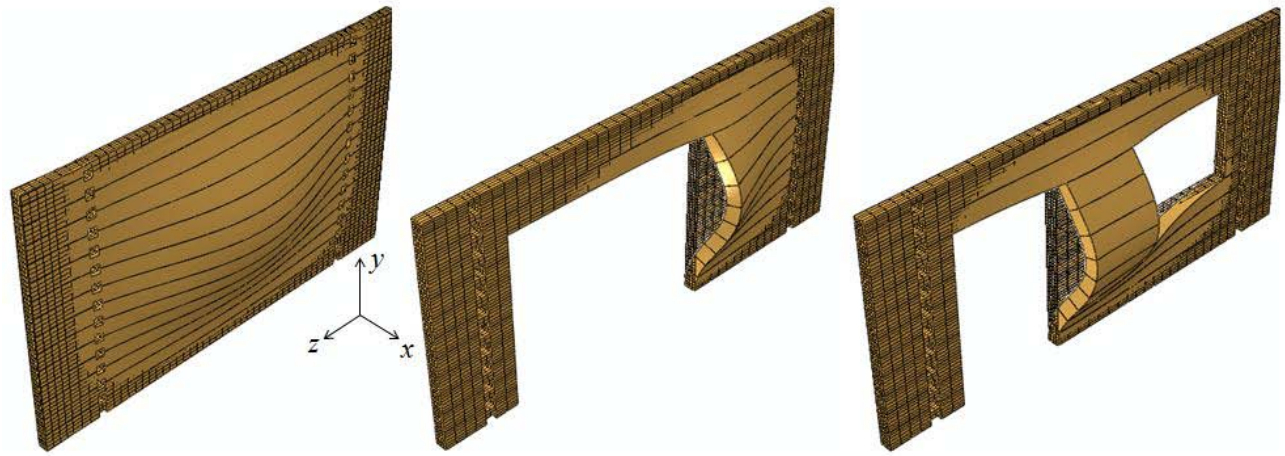

(a) (b) (c)

Fig.9. Fundamental modal shapes obtained from preliminary FE-models (ABAQUS *eb*) for log-wall specimens (a) without openings (type A04); (b) with single door opening (type B02) and (c) with double openings (type B04). RTL boundary condition.

Figure 10

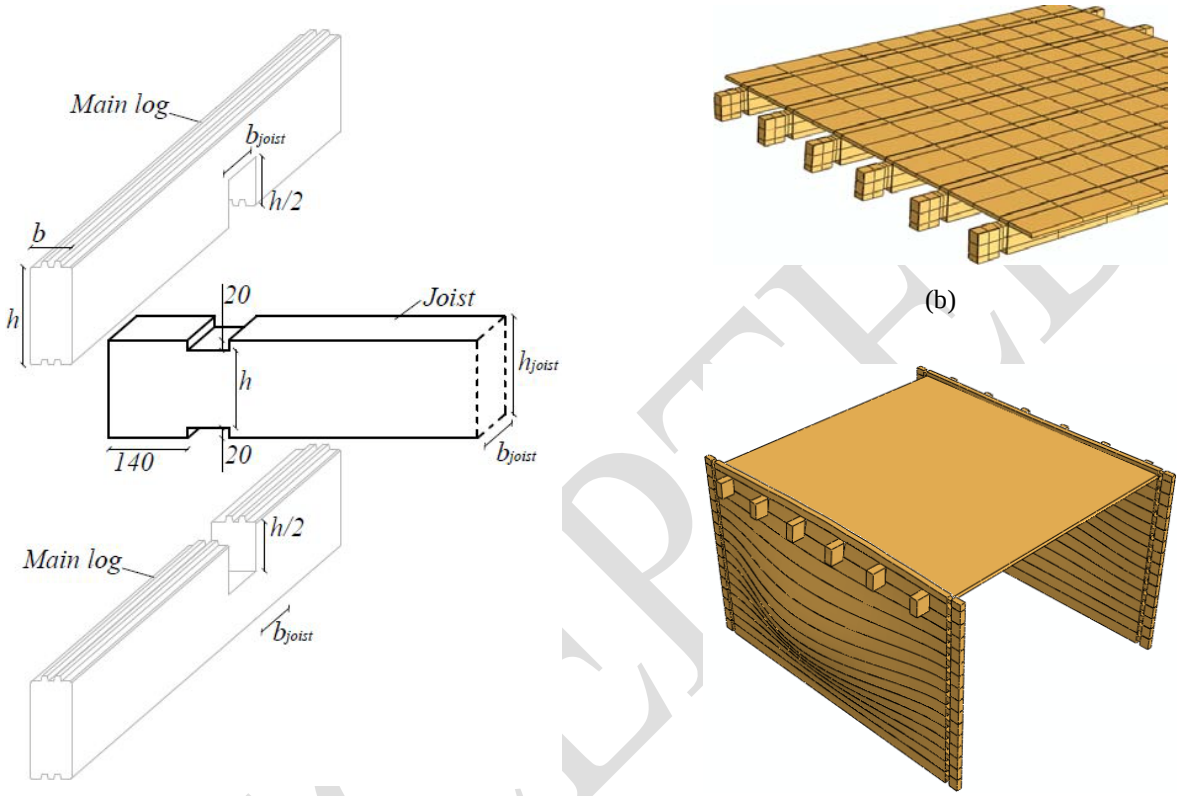

Fig.10. Example of typical inter-storey floor of *Blockhaus* structural systems.
(a) detail of joist-to-wall connection (exploded axonometric view), nominal dimensions in mm;
(b) FE-model detail (ABAQUS *eb*); (c) fundamental modal shape (ABAQUS *eb*).

Figure 11

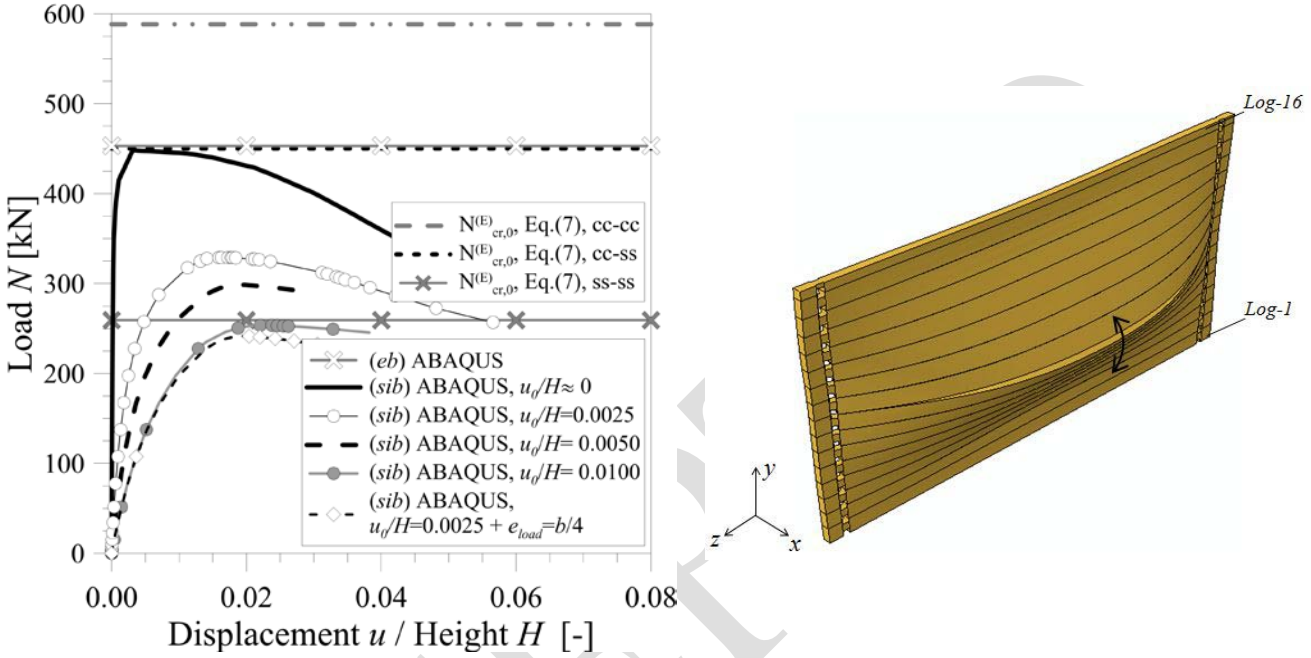

(a) (b)

Fig.11. Effect of initial curvatures u_0 or load eccentricities e_{load} (ABAQUS-RTL *sib*). 'Tirol' log-wall with L= 4m and H= 2.945m. (a) Load N-maximum transversal displacement u, compared to Euler's critical loads given by Eq.(7) for log-walls with all edges simply supported (*ss-ss*, k_σ= 4); lateral clamps and top-bottom supports (*cc-ss*, k_σ= 6.97), all edges clamped (*cc-cc*, k_σ= 8.93); (b) example of deformed shape at failure.

Figure 12

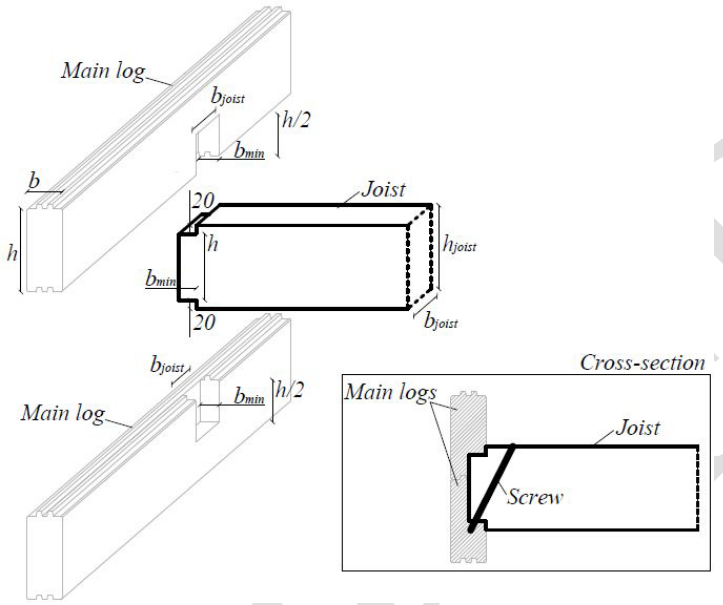

Fig.12. Example of eccentric joist-to-wall connection between an inter-storey floor and the main wall (exploded axonometric view), nominal dimensions in mm

Figure 13

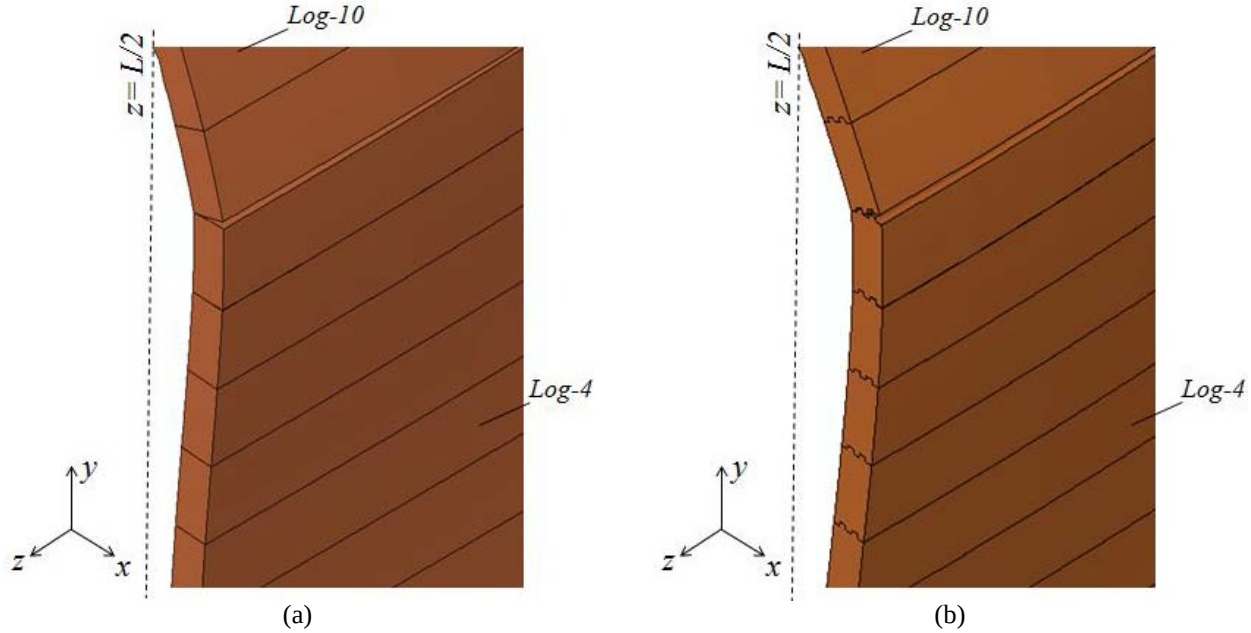

(a) (b)

Fig.13. Effect of geometrical description of log profiles on the buckling behaviour of *Blockhaus* walls (ABAQUS-RTL *sib*). (a) *b*×*h* cross-section; (b) nominal profile with protrusions and tongues.

Figure 14

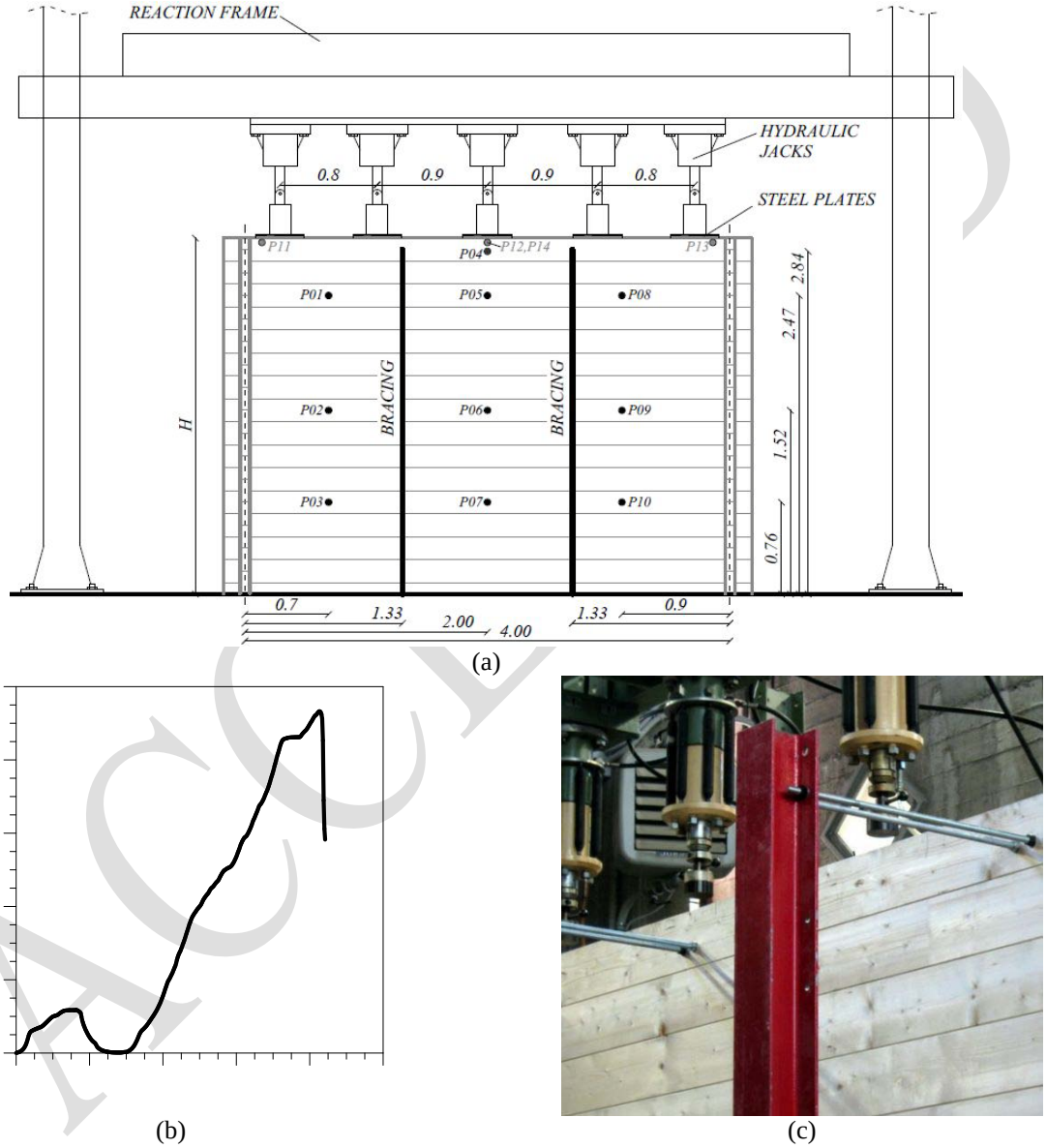

Fig.14. Experimental setup for full-scale buckling experiments.
(a) Elevation of specimens with position of instrumentation (nominal dimensions in m). Black and grey dots denote the position of transducers for out-of-plane and vertical deflections respectively; (b) typical load N – time history; (c) detail of connection between the top log of specimens and the metal bracings.

Figure 15

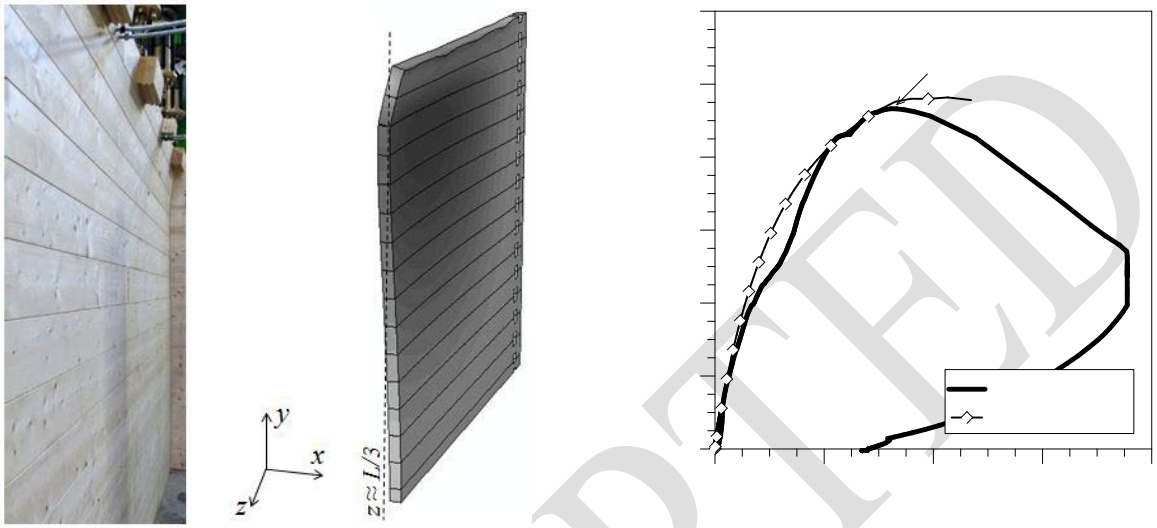

(a) (b) (c)

Fig.15. Full-scale buckling experiments (specimen LW01). (a) Deformed shape of specimen, greyscale contour plot of maximum displacements; (b) detail of ABAQUS deformed shape; (c) comparison between *N*-*u* test measurements and corresponding numerical predictions (ABAQUS *sib*), $e_{load} \approx b/2$.

Figure 16

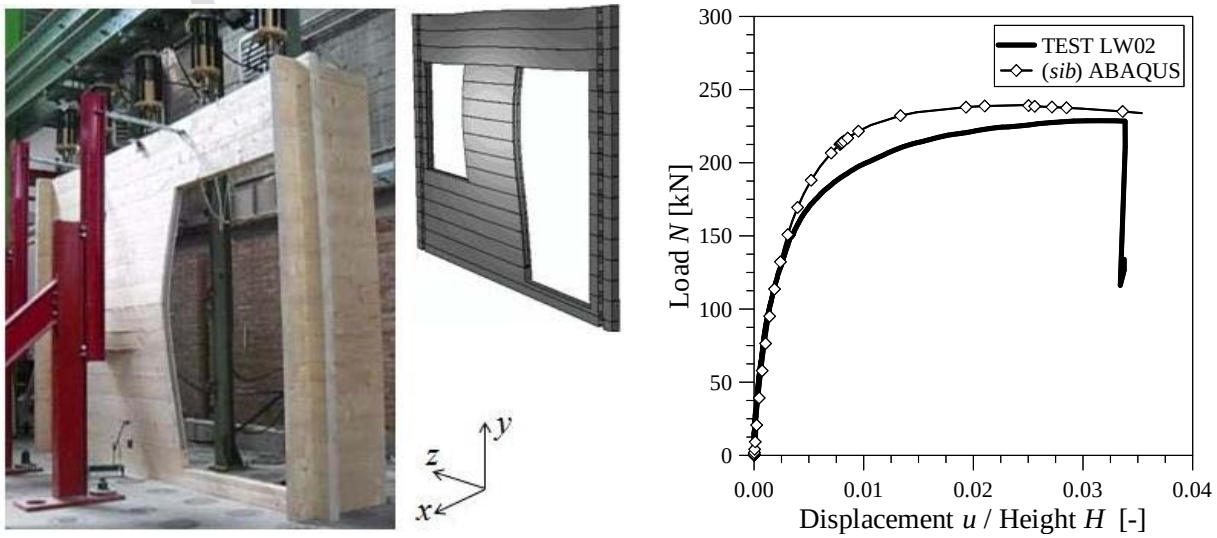

(a) (b)

Fig.16. Full-scale buckling experiments (specimen LW02). (a) Deformed shapes obtained from the experiment and ABAQUS FE-model; (b) Comparison between *N*-*u* test measurements (control point P06) and corresponding numerical predictions (ABAQUS *sib*), $e_{load} \approx b/5$.

Figure 17

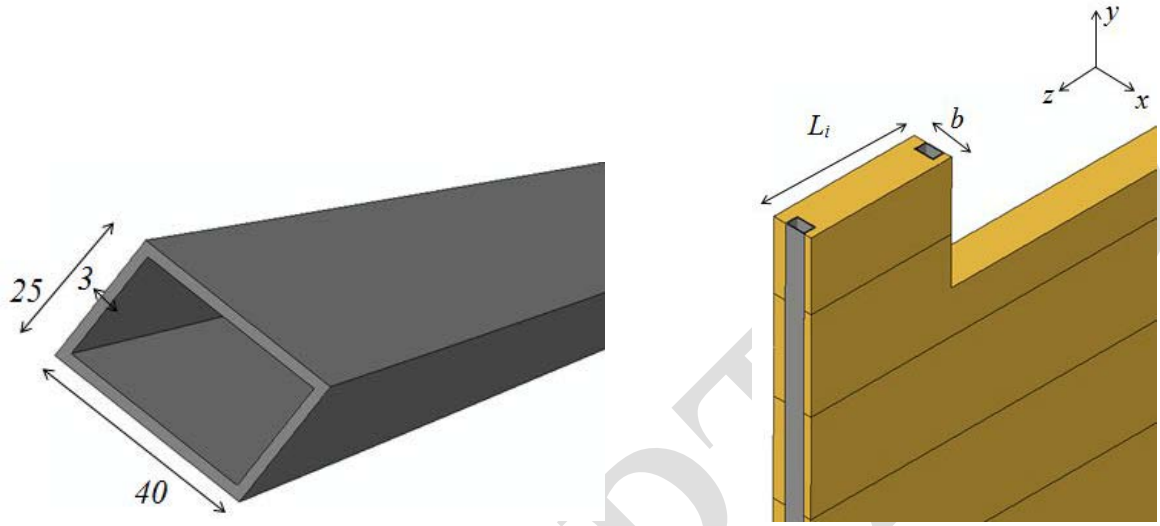

(a) (b)

Fig.17. Detail of FE-model for the LW02 specimen. (a) metal stiffener (dimensions in mm) and (b) elevation of the wall showing the position of the stiffeners along the vertical edges of openings

Figure 18

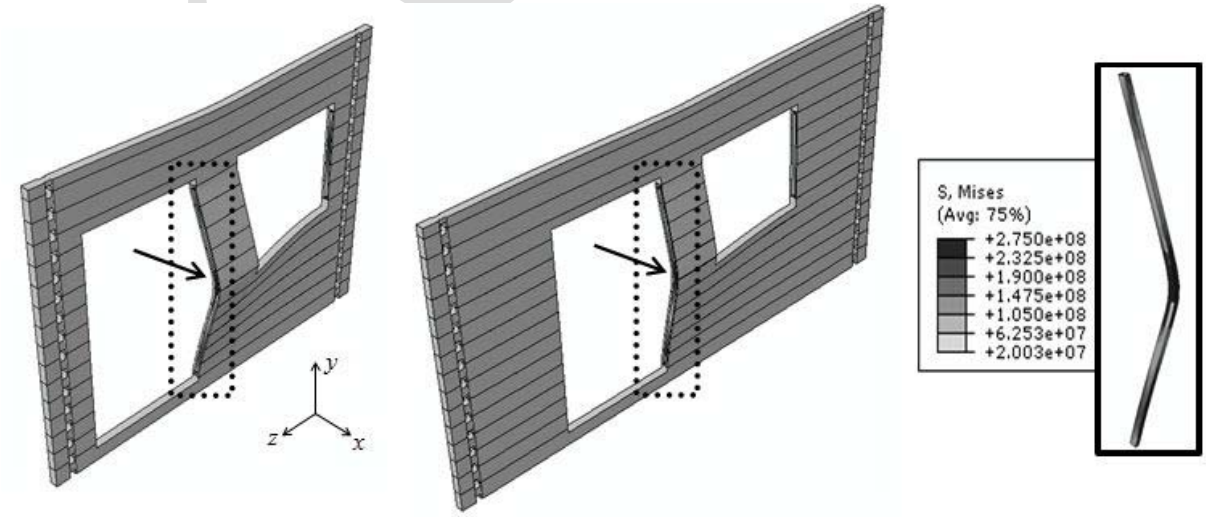

(a) (b) (c)

Fig.18. Typical buckling failure configuration for log-walls with double opening (ABAQUS *sib*).
(a) FE-model W2-3.5-0.5; (b) FE-model W2-5-0.5; (c) detail of yielding in the central metal stiffener.

Figure 19

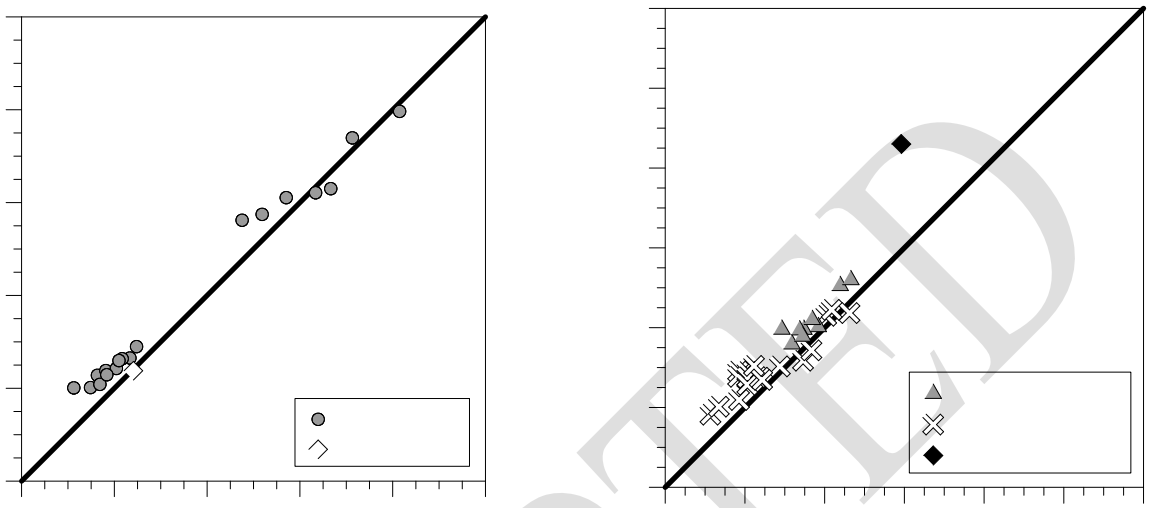

(a) (b)

Fig.19. Comparison of numerical (ABAQUS *sib*) and analytical (Eq.(15)) design buckling resistances $N_{b,Rd}$ for log-walls with no, single or double openings ($0.001 \leq u_0/H \leq 0.005$ and $0 \leq e_{load} \leq b/2$).

(a) No openings; (b) 'Tirol' log-walls with single or double door openings.

Table 1

Table 1. Comparison between experimental [4, 5], numerical (ABAQUS *eb*) and analytical critical buckling loads $N_{cr,0}^{(E)}$ for specimens without openings, with single door opening or with double door / window openings. [(i)] Eq.(2); [(ii)] Eq.(3); [(iii)] Eq.(4).

		Experimental [4, 5]		Predicted (UTL)		
Specimen type	N.° of openings	N.° of specimens	Average ± St.Dev. [kN]	Numerical *eb* [kN]		Analytical [kN]
				FE-model with outriggers	*FE-model with equivalent boundaries*	
A01	-	4	9.9 ± 1.4	11.1	11.2	5.7 [(i)]
A04	-	2	15.1 ± 3.3	15.8	15.9	8.9 [(i)]
B01	-	3	202.0 ± 47.3	181.8	182.7	133.6 [(i)]
A02	1	4	8.5 ± 1.3	6.0	6.1	3.4 [(ii)]
A05	1	2	16.4 ± 1.2	10.8	10.9	5.5 [(ii)]
B02	1	3	82.5 ± 9.4	82.1	82.9	48.9 [(ii)]
A03	2	4	10.2 ± 2.2	5.8	5.9	2.4 [(iii)]
B04	2	3	89.9 ± 6.8	89.2	91.1	37.8 [(iii)]

Table 2

Table 2. Numerical (ABAQUS *eb* and *sib*) and analytical (Eq.(7)) predictions of Euler's critical loads $N_{cr,0}^{(E)}$ and buckling failure loads N_{max} (u_0/H= 0.0025) for log-walls without openings.
ss-ss= all edges simply supported, [(i)] k_σ= *f(H/L)*; [(ii)] k_σ= 4.
cc-ss= clamped lateral edges and simply supported top-bottom edges, [(i)] k_σ= *f(H/L)*; [(ii)] k_σ= 6.97.
$\Delta_1 = 100 \cdot \left(N^{eb} - N^{ss-ss^{(i)}}\right) \Big/ N^{ss-ss^{(i)}}$, $\Delta_2 = 100 \cdot \left(N^{eb} - N^{ss-ss^{(ii)}}\right) \Big/ N^{ss-ss^{(ii)}}$, $\Delta_3 = 100 \cdot \left(N^{eb} - N^{cc-ss^{(i)}}\right) \Big/ N^{cc-ss^{(i)}}$,
$\Delta_4 = 100 \cdot \left(N^{eb} - N^{cc-ss^{(ii)}}\right) \Big/ N^{cc-ss^{(ii)}}$, $\Delta_5 = 100 \cdot \left(N^{eb} - N^{sib}\right) \Big/ N^{sib}$.

		Critical buckling load $N_{cr,0}^{(E)}$									Ultimate buckling load N_{max}	
FE-model	*H/L*	ABAQUS *eb*	Analytical (Eq.(7))								(ABAQUS *sib*) u_0/H=0.0025	
			ss-ss [(i)]		*ss-ss* [(ii)]		*cc-ss* [(i)]		*cc-ss* [(ii)]			
		[kN]	[kN]	Δ_1 [%]	[kN]	Δ_2 [%]	[kN]	Δ_3 [%]	[kN]	Δ_4 [%]	[kN]	Δ_5 [%]
W0-0.08-6.0	0.491	326.65	270.86	*20.6*	172.23	*89.7*	339.44	*-3.8*	300.11	*8.8*	226.30	*44.3*
W0-0.08-5.5	0.535	337.40	266.17	*26.8*	187.89	*79.6*	342.67	*-1.5*	327.39	*3.1*	274.70	*22.8*
W0-0.08-5.0	0.589	356.09	265.72	*34.0*	206.68	*72.3*	365.78	*-2.6*	360.13	*-1.1*	284.90	*24.9*
W0-0.08-4.5	0.654	391.14	270.00	*44.9*	229.64	*70.3*	402.24	*-2.8*	400.15	*-2.3*	295.14	*32.5*
W0-0.08-4.0	0.736	453.11	280.93	*61.3*	259.35	*74.7*	458.30	*-1.1*	450.17	*0.7*	311.60	*45.4*
W0-0.08-3.5	0.841	490.85	303.17	*61.9*	295.25	*66.3*	554.48	*-11.5*	514.48	*-4.6*	337.05	*45.6*
W0-0.12-6.0	0.491	1087.59	914.16	*19.0*	581.28	*87.1*	1145.61	*-5.1*	1012.88	*7.4*	756.25	*43.8*
W0-0.12-5.5	0.535	1178.54	898.32	*31.2*	634.12	*62.6*	1156.52	*1.9*	1104.96	*6.7*	804.11	*46.5*
W0-0.12-5.0	0.589	1203.32	896.80	*34.2*	697.53	*58.2*	1234.50	*-2.5*	1215.45	*-1.0*	854.50	*40.9*
W0-0.12-4.5	0.654	1242.16	911.26	*36.3*	775.04	*60.3*	1357.57	*-8.5*	1350.50	*-8.0*	883.12	*40.7*
W0-0.12-4.0	0.736	1516.58	948.13	*60.0*	871.92	*73.9*	1546.75	*-2.0*	1519.31	*-0.2*	930.64	*62.8*
W0-0.12-3.5	0.841	1682.54	1023.20	*64.4*	996.48	*68.8*	1871.38	*-10.1*	1736.36	*-3.1*	988.10	*70.2*

Table 3

Table 3. Numerical (ABAQUS *eb* and *sib*) and analytical (Eq.(7)) predictions of Euler's critical loads $N_{cr,0}^{(E)}$ and buckling failure loads N_{max} (u_0/H= 0.0025) for log-walls with single door opening.
cf-ss= one clamped and one free lateral edges, with simply supported top-bottom edges (k_σ= 1.277).
$\Delta_1 = 100 \cdot \left(N^{eb,steel} - N^{eb} \right) / N^{eb}$, $\Delta_2 = 100 \cdot \left(N^{eb,steel} - N^{cf-ss} \right) / N^{cf-ss}$, $\Delta_3 = 100 \cdot \left(N^{eb,steel} - N^{sib,steel} \right) / N^{sib,steel}$.

		Critical buckling load $N_{cr,0}^{(E)}$					Ultimate buckling load N_{max}	
		ABAQUS *eb* With profiles	ABAQUS *eb* without profiles	Δ_1	Analytical (Eq.(7))		(ABAQUS *sib*, with profiles) u_0/H=0.0025	
FE model	H/L_{ef} [-]	[kN]	[kN]	[%]	*cf-ss* [kN]	Δ_2 [%]	[kN]	Δ_3 [%]
W1-6.0-3.11	0.934	173.16	163.33	*6.0*	106.08	*63.2*	142.36	*21.6*
W1-5.5-2.90	1.015	177.71	168.05	*5.8*	113.76	*56.2*	154.02	*15.4*
W1-5.0-2.65	1.111	188.16	172.71	*8.9*	124.49	*51.1*	159.05	*18.3*
W1-4.5-2.36	1.247	200.55	192.30	*4.3*	139.79	*43.5*	170.02	*17.9*
W1-4.0-2.11	1.395	220.98	208.82	*5.8*	156.35	*41.3*	183.51	*20.4*
W1-3.5-1.90	1.550	238.51	228.29	*4.5*	173.64	*37.4*	195.05	*22.2*

Table 4

Table 4. Numerical (ABAQUS *eb* and *sib*) and analytical (Eq.(8)) predictions of Euler's critical loads $N_{cr,0}^{(E)}$ and buckling failure loads N_{max} (u_0/H= 0.0025) for log-walls with double door/window openings.
[i] β= *0.7;* [ii] β= *1*

$\Delta_1 = 100 \cdot \left(N^{eb,steel} - N^{eb} \right) / N^{eb}$, $\Delta_2 = 100 \cdot \left(N^{eb,steel} - N^{(i)} \right) / N^{(i)}$, $\Delta_3 = 100 \cdot \left(N^{eb,steel} - N^{(ii)} \right) / N^{(ii)}$,
$\Delta_4 = 100 \cdot \left(N^{eb,steel} - N^{sib,steel} \right) / N^{sib,steel}$.

	Critical buckling load $N_{cr,0}^{(E)}$							Ultimate buckling load N_{max}	
	ABAQUS *eb* With profiles	ABAQUS *eb* Without profiles	Δ_1	Analytical (Eq.(8)) With profiles				(ABAQUS *sib*, with profiles) u_0/H=0.0025	
FE model				*clamp-pin* [i]		*pin-pin* [ii]			
	[kN]	[kN]	[%]	[kN]	Δ_2 [%]	[kN]	Δ_3 [%]	[kN]	Δ_4 [%]
W2-6.0-3.2	228.36	212.23	*7.6*	286.62	*-20.3*	140.04	*63.1*	165.60	*37.1*
W2-5.5-2.7	225.17	203.31	*10.8*	254.56	*-11.5*	124.38	*81.0*	171.20	*31.5*
W2-5.0-2.2	222.52	193.19	*15.2*	222.49	*0.1*	108.71	*104.7*	184.30	*20.7*
W2-4.5-1.7	199.41	167.68	*18.9*	190.43	*4.7*	93.05	*114.3*	126.97	*57.1*
W2-4.0-1.2	186.67	153.90	*21.3*	158.37	*17.9*	77.38	*141.2*	117.15	*59.3*
W2-3.5-0.7	182.76	145.73	*25.4*	126.31	*44.7*	61.71	*196.2*	106.40	*71.8*
W2-6.0-0.3	155.51	121.89	*27.6*	100.66	*54.5*	49.18	*216.2*	101.10	*53.8*
W2-5.5-0.3	163.27	122.39	*33.4*		*62.2*		*232.0*	105.35	*55.0*
W2-5.0-0.3	159.99	121.51	*31.7*		*58.9*		*225.3*	103.15	*55.1*
W2-4.5-0.3	163.81	117.81	*39.0*		*62.7*		*233.1*	106.55	*53.7*
W2-4.0-0.3	168.24	124.61	*35.0*		*67.1*		*242.1*	103.25	*62.9*
W2-3.5-0.3	164.63	114.26	*44.1*		*63.6*		*234.7*	104.50	*57.7*
W2-6.0-0.5	169.80	148.18	*14.6*	113.48	*49.6*	55.45	*206.2*	118.85	*42.9*
W2-5.5-0.5	174.24	151.73	*14.8*		*53.5*		*214.2*	119.02	*46.4*
W2-5.0-0.5	181.32	154.02	*17.7*		*59.8*		*227.0*	114.25	*58.7*
W2-4.5-0.5	187.88	152.74	*23.0*		*65.6*		*238.8*	115.30	*62.9*
W2-4.0-0.5	191.62	152.30	*25.8*		*68.9*		*245.6*	113.22	*69.2*
W2-3.5-0.5	195.68	149.59	*30.8*		*72.4*		*252.9*	117.35	*66.7*